# Bursting firing in ventromedial hypothalamic neurons exerts dual control of anxiety-like behavior and energy expenditure

Jie Shao[1,2,4], Dashuang Gao[1,2,4], Yunhui Liu[1,2,4], Shanping Chen[1], Nian Liu[1], Lu Zhang[1], Xinyi Zhou[1,2], Qian Xiao[1,2], Liping Wang[1], Hailan Hu[3], Fan Yang[1,5,*]

[1]The Brain Cognition and Brain Disease Institute, Shenzhen Institutes of Advanced Technology, Chinese Academy of Sciences, Shenzhen-Hong Kong Institute of Brain Science-Shenzhen Fundamental Research Institutions, Shenzhen 518055, China.

[2]University of Chinese Academy of Sciences, Beijing 100049, China.

[3]Department of Psychiatry of First Affiliated Hospital, Zhejiang University School of Medicine, Hangzhou 310058, China.

[4]These authors contributed equally.

[5]Lead contact

*Correspondence to: Fan Yang, Shenzhen Institutes of Advanced Technology, Chinese Academy of Sciences, 1068 Xueyuan Boulevard, University Town of Shenzhen, Xili Nanshan, Shenzhen 518055, China. Email: fan.yang@siat.ac.cn;

**Abstract**

Exposure to chronic stress induces anxiety-like behavior and metabolic changes in animals, resulting in adaptive or maladaptive responses to the stressful environment. Recent studies have indicated the dorsomedial ventromedial hypothalamus (dmVMH) as an important hub that regulates both anxiety and energy homeostasis. However, up to now, how dmVMH neurons exert dual control of chronic stress-induced anxiety and energy expenditure remains poorly understood. Here, we established a chronic-stress mouse model that induced anxiety-like behavior, reduced food consumption, and decreased energy expenditure. We found that *c-fos* expression increased and theta band power is higher in the dmVMH after chronic stress, and the proportion of burst firing neurons significantly increased, which was mediated by elevated expression of T-type calcium channel Cav 3.1. Optogenetically evoked burst firing of dmVMH neurons induced anxiety-like behavior, shifted the respiratory exchange ratio toward fat oxidation, and decreased food intake, while knockdown of Cav3.1 in the dmVMH had the opposite effects. Collectively, our study first revealed an important role of dmVMH burst firing in the dual regulation of anxiety-like behavior and energy expenditure, and identified Cav 3.1 as a crucial regulator of the activity of the burst firing neurons in dmVMH. These molecular and cellular level findings will advance our understanding of the chronic stress-induced emotional malfunction and energy expenditure disorders.

**Keywords:** Chronic stress; VMH; Burst firing; Anxiety; Energy expenditure

## Introduction

Exposure to stressors regulate neural activity that integrate the aversive behavior and energy expenditure to facilitate stress coping and survival[1-3], however long-term stress causes adverse effects, impairing both mental and physiological functions [4,5] including anxiety-like behavior [6,7] and metabolic malfunctions in glucose [8,9] and lipid tissues [3,10]. Particular effort has been expended to identify the crucial central nodes that interconnect the regulation of emotion and metabolic processes [3,9,11]. The hypothalamus, especially the ventromedial hypothalamus (VMH), has been found to play crucial roles in controlling both innate survival behaviors [12,13] and energy homeostasis [11,14,15].

The VMH is an evolutionarily conserved deep subcortical nucleus[16]. While the ventrolateral part (vl) of the VMH modulates a series of social behaviors [17-19], the dorsomedial part (dm) is specifically involved in maintaining energy homeostasis [14,15,20,21] and stress response[13,22]. Oscillations in the dmVMH can act on sympathetic excitation and regulate energy expenditure [23,24]. Steroidogenic factor-1 (SF-1) -expressing neurons are enriched in the dmVMH and play important roles in controlling food intake and energy expenditure [14,15,20,21]. Optogenetic activation of VMH SF-1 neurons induces aversive behavior in mice [13,22]. Furthermore, SF-1 neurons can act as a nutrient-sensitive switch between feeding and anxiety states when facing potential stresses [2]. Given the complicated functions of SF-1 neurons [19], it is important to dissect how molecular or electrophysiological distinct neuronal subtypes regulate

62 emotional state and energy homeostasis. However up to now, how dmVMH neurons
63 control neuronal firing to regulate chronic stress-induced anxiety and energy metabolic
64 disorders is elusive.
65
66 Recent studies have demonstrated the role of burst firing neurons in regulating
67 emotional state and brain functions; neuronal burst firing and oscillation are critical for
68 the transmission of information and regulation of specific physiological processes in
69 crucial brain areas[25-30]. In the hippocampus, burst firing of CA1 pyramidal neurons play
70 an important role in regulating N-methyl-d-aspartate (NMDA)-mediated transmission
71 and the epileptogenic mechanism [25]. In the ventral subiculum, chronic social defeat
72 stress increases both T-type calcium channel (T-VGCC)-mediated currents and
73 expression of Cav3.1 protein [29]. In the lateral habenula, NMDA-receptor-and- T-VGCC
74 -dependent bursting activity are increased after chronic stress and, most strikingly, can
75 drive depression-like behaviors [26]. Based on these evidences, we decided to investigate
76 the specific function of bursting firing in the dmVMH, and whether it may be involved
77 in chronic stress-induced anxiety-like behavior and energy metabolic changes.
78
79 In this study, we first identified that dmVMH neurons can be classified into silent,
80 tonic-firing, and bursting subtypes. We also established a chronic-stress mouse model
81 that induced anxiety-like behavior, reduced food consumption, and decreased energy
82 expenditure. We found a significantly increased proportion of bursting neurons under

83 chronic stress conditions, which was mainly caused by elevated T-type calcium channel
84 Cav3.1 expression. Importantly, optogenetically-induced dmVMH burst firing drive
85 anxiety-like behaviors, shifted respiratory exchange ratio and decreased average
86 energy expenditure in naïve mice. Conversely, knockdown of Cav3.1 in the dmVMH
87 rescued chronic stress-induced anxiety-like behavior and energy expenditure changes.
88 Taken together, our study first identified Cav3.1-mediated burst firing pattern in the
89 dmVMH, and demonstrated its crucial role in regulating anxiety-like behavior and
90 energy expenditure during the chronic stress.
91

92 **Results**

93 **Chronic stressors induced anxiety-like behavior and energy expenditure change**

94 Repeated exposure to stressors modifies the activity of neuronal circuits associated
95 with a variety of abnormalities, including behavior, emotional state, and energy
96 expenditure [2], which adaptively or maladaptively respond to the stressful situation. To
97 probe the impact of chronic stress on behavior and energy metabolism, we applied
98 unpredictable chronic stressors to establish a stress mouse model. During the chronic
99 stress period, mice were exposed to random stressors for four weeks, as illustrated in
100 Fig. 1a, with no stressors used in the control group. Both the wild-type and stress
101 groups were tested in a comprehensive phenotyping paradigm. Consistent with
102 previous reports [6,7], we found that chronic stress induced a state of anxiety (Fig. 1b-e).
103 Compared with the control group, mice in the stress group spent less time in the central

area of the open field and open arm of the elevated plus maze without any change in locomotion distance (Fig. 1c and e). The number of entries into the central area and open arms also decreased in the stress group compared with the control group (Fig. 1c and e).

We next explored whether chronic stress affected energy expenditure in stressed mice. The body weight of each mouse was measured after the chronic stress period, and no significant difference was observed between the control and stress groups (Fig. 1f). Both the respiratory exchange ratio (RER) and food intake were monitored for 24 h using comprehensive laboratory animal monitoring system (CLAMS) cages. Results showed that the average RER of the stress group was much lower than that of the control group, which represented a shift toward fat oxidation (Fig. 1g). Energy expenditure was calculated from oxygen consumption and RER. Average energy expenditure also showed a significant decrease in stressed mice (Fig. 1h). To determine the underlying cause of different RER in the treatment groups, we also analyzed food intake. As expected, caloric intake in stressed mice was significantly lower than that in the controls, consistent with the known effects of anxiety on food intake (Fig. 1f). Taken together, these findings suggest that chronic stress can induce anxiety-like behavior, reduce food consumption, and shift the RER toward fat oxidation.

Given its important role in regulating anxiety, feeding, and energy expenditure [2,21], we

125 hypothesized that the dmVMH may be involved in the above chronic stress-induced
126 changes. After chronic stress, mice were perfused, and *c-fos* expression was determined
127 via immunostaining. Higher *c-fos* expression was found in the dmVMH of chronically
128 stressed mice than in that of the control group (Fig. 1i), suggesting that more dmVMH
129 neurons were activated under chronic stress conditions. We then employed *in vivo*
130 electrophysiology to record neuronal activity in the dmVMH. Mice were implanted
131 with Ni-Cr electrodes into the dmVMH after chronic stress induction (Fig. 1j), and
132 dmVMH neuronal activity was monitored after recovery from surgery. The local field
133 potential (LFP) results demonstrated that stressed mice exhibited higher theta band
134 power in the dmVMH than that of control mice (Fig. 1k-l). Together with the *c-fos*
135 staining results, our data suggest that dmVMH neuronal activity is significantly
136 changed after chronic stress.
137
138 **Chronic stressors induced burst firing in dmVMH**
139 The above experiments revealed enhanced neuronal activity in the dmVMH under
140 chronic stress, but the underlying mechanism was unclear. To explore which
141 electrophysiological characteristics of dmVMH neurons changed after chronic stress,
142 we recorded 84 dmVMH neurons from 38 stressed mice and 85 dmVMH neurons from
143 32 control mice under whole-cell patch clamp configuration and analyzed the
144 electrophysiological characteristics. Our data demonstrated that these neurons
145 displayed shorter onset time and depolarized RMP, on average, compared with the

146 control group (Fig. 1a). The alterations implied that the overall excitability of dmVMH
147 neurons was enhanced under chronic stress, consistent with the *c-fos* immunostaining
148 and *in vivo* electrode recording results.
149
150 We carried out a comprehensive analysis of the membrane properties of dmVMH
151 neurons to quantitatively determine their electrophysiological diversity (Fig. 2b). To
152 classify these neurons, we measured and analyzed eight electrophysiological
153 parameters (Table 1) and performed cluster analysis. The resulting dendrogram in Fig.
154 2b (with rescaled distance shown along the vertical axis) illustrates the similarity
155 between clusters. Furthermore, cluster analysis showed that all neurons could be
156 divided into three subtypes: i.e., silent, tonic-firing, bursting. These three dmVMH
157 neuronal subtypes displayed distinct electrophysiological properties (Fig. 2b, Extended
158 Data Fig. 1).
159
160 We then applied cluster analysis using the same methods as depicted above (Fig. 2d) to
161 explore overall changes in the electrophysiological properties of dmVMH neurons after
162 chronic stress. We found that dmVMH neurons in stressed mice could also be divided
163 into three subtypes. Onset time, RMP and recording site of these three subtypes were
164 also compared with those of the control group (Extended Data Fig. 2). By analyzing
165 data from behavior tests and electrophysiological recordings, we found the proportion
166 of burst firing neurons in stressed group, especially in mice with obvious anxiety-like

167 behavior (anxiety group), increased significantly compared with that in the control
168 group, whereas the proportion of the other subtypes decreased (Fig. 2d-e). This
169 alteration could explain why dmVMH neurons from stressed mice demonstrated a
170 shorter average onset time of action potentials induced by 50 pA current injection (Fig.
171 2a), as burst firing neurons displayed a similar onset time as tonic-firing neurons but a
172 shorter onset time compared with silent neurons (Fig. 2f, Extended Data Fig. 2b). In
173 addition, the increased proportion of bursting neurons and more depolarized
174 tonic-firing neurons (Fig. 2f, Extended Data Fig. 2a) may have contributed to the higher
175 average RMP in dmVMH neurons after chronic stress (Fig. 2a). Furthermore, the
176 average inter-spike interval (ISI, between first and second spike of a burst) of dmVMH
177 burst firing neurons in anxiety group was shorter than that of the control group
178 (unpaired Student's *t*-test, $P = 0.0173$), and a shorter ISI represents higher frequency
179 firing in a single burst (Fig. 2g). We also found that ISI of dmVMH bursting neurons
180 was more correlated with the time in central area or open arms in mice of
181 stress-induced anxiety compared with the mice in control group (Fig. 2h,i). Taken
182 together, these results demonstrate a possible link between increased bursting activity
183 in the dmVMH and chronic stress induced anxiety.
184

185 **Optogenetic manipulation of burst firing neurons in dmVMH**

186 Given the enhancement of burst firing in the dmVMH after chronic stress, we
187 investigated whether induced burst firing of dmVMH neurons alone in unstressed mice

188 was sufficient to produce a similar response in behavior and energy metabolism. We
189 first applied optogenetic manipulation to elicit a low-threshold spike and mimic the
190 generation of bursting in dmVMH neurons (Fig. 3a). *In vitro* patch clamp experiments
191 on brain slices indicated that yellow light illumination at 0.1 Hz could slightly
192 hyperpolarize and depolarize bursting neurons periodically, which enabled the
193 re-activation of calcium channels and generation of burst firing during the light
194 "ON-OFF" intervals in bursting neurons (Fig. 3b). The evoked burst firing did not
195 follow the "ON-OFF" intervals when the illumination frequency was over 0.1 Hz (Fig.
196 3b). In addition, illumination at 0.1 Hz exerted no significant effects on the tonic-firing
197 or silent neuronal subtypes (Fig. 3c).
198
199 We then applied low-frequency yellow light illumination to induce burst firing *in vivo*
200 and performed behavioral and energy metabolic tests in NpHR-expressing mice (Fig.
201 3d). This led to decreased residence time in the central area of the open field and open
202 arm of the elevated plus maze, mimicking the effects of chronic stress-induced
203 anxiety-like behavior (Fig. 3e,f). We also applied wireless optogenetics to induce burst
204 firing of neurons and simultaneously monitored the metabolism of mice using CLAMS.
205 We applied 0.1-Hz yellow light illumination at the start of the test period for 2 h and
206 repeated the stimulation after 12 h, with consecutive monitoring of mouse energy
207 metabolism for 24 h. Results indicated that average RER, energy expenditure, and food
208 intake in the test period decreased significantly compared with the baseline level before

209 the test period (Fig. 3g-i). Taken together, our results indicated that enhancement of
210 burst firing induced by local optogenetic manipulation in the dmVMH was sufficient to
211 affect anxiety-like behavior and energy expenditure changes, which simulated the
212 phenotypes of chronically stressed mice.
213
214 **Burst firing in dmVMH is mediated by T-VGCC**
215 Bursting is an important firing pattern in neural systems and is essential for specific
216 information transmission and function regulation[30]. The T-VGCC, including its three
217 isoforms (Cav3.1, Cav3.2, and Cav3.3), is a pacemaker that can generate LTS [26,31].
218 Unlike hyperpolarization-activated cyclic nucleotide-gated channel (HCN), the
219 T-VGCC can induce higher frequency firing and has a threshold near to RMP. It has
220 been reported that Cav 3.1 and Cav 3.2 alone display strong burst firing with a
221 low-voltage threshold, whereas Cav3.3 contributes to burst firing in a different way [31].
222 The expression of T-VGCC is highly correlated with T-type calcium currents, which
223 directly affect the strength and width of bursting [29,32]. Given the known role of T-VGCC
224 in burst firing, we examined T-VGCC expression in the dmVMH after chronic stress.
225
226 Based on immunohistochemical analysis, Cav3.1, Cav3.2, and Cav3.3 were all found to
227 be expressed in the dmVMH of naïve mice. The signals of Cav3.1 were much stronger
228 than those of Cav3.2 and Cav3.3 (Fig. 4a). To investigate whether differential
229 expression of the T-VGCC occurs after chronic stress, we performed acute dissection of

230 dmVMH tissue from brain slices and harvested single dmVMH cells after patch
231 recordings to extract RNA, then performed qRT-PCR to quantify T-VGCC expression.
232 The expression of Cav3.1 in the dmVMH of stressed mice was significantly higher than
233 that of the control group, whereas no obvious changes were observed in Cav 3.2 or Cav
234 3.3 at either the tissue or single-cell level (Fig. 4b-c).
235
236 To further confirm the contribution of the T-VGCC in dmVMH burst generation, we
237 applied mibefradil, an antagonist of T-VGCC, in whole-cell recording experiments.
238 Results indicated that the burst firing of dmVMH neurons elicited by a 10-pA current
239 injection was indeed inhibited (Fig. 4d). Furthermore, we found that application of
240 mibefradil increased the onset time in the dmVMH neurons of the stress group, but not
241 in the control group, but the change in RMP was similar between the two groups (Fig.
242 4e). Moreover, as we collected single neurons after whole-cell recordings for T-VGCC
243 quantification, we combined the single-cell qRT-PCR and electrophysiological
244 classification data to determine the differential expression of Cav3.1 in the dmVMH
245 neuronal subtypes. Results showed that Cav3.1 expression was much more enriched in
246 dmVMH bursting neurons, especially after chronic stress (Fig. 4f). Consistently, the
247 Cav3.2 antagonist ascorbate [33] did not significantly affect burst firing of dmVMH
248 neurons (Extended Data Fig. 3). We also investigated the effects of mibefradil on the
249 frequency-current curves using the same stimulus protocol, and found that the firing
250 rate of bursting neurons was decreased by bath application of mibefradil($P$ = 0.007, Fig.

251 4g, right), but the changes in the firing rate were much more significant in the stress
252 group than in the control group ($P = 0.0047$, Fig. 4h, upper). These data support the idea
253 that the T-VGCC, especially the Cav3.1 isoform, mediates burst firing in the dmVMH.
254
255 To investigate the *in vivo* effects of T-VGCC blockade, we bilaterally implanted a
256 cannula and precisely delivered mibefradil or saline into the dmVMH of chronically
257 stressed mice to block burst firing (Extended Data Fig. 4a). Results showed that
258 mibefradil infusion increased the time spent in the central area of the open field and
259 open arm of the elevated plus maze compared with the control group treated with saline
260 (Extended Data Fig. 4b). We also investigated energy metabolic changes after oral
261 administration of mibefradil, and found it to have no effect on food intake. However,
262 administration of mibefradil significantly rescued the decreased RER found in stressed
263 mice. Taken together, these data indicate that the T-VGCC in the dmVMH mediates
264 chronic stress-induced behavioral and energy expenditure changes.
265
266 The function of the T-VGCC is tightly related to postsynaptic excitatory/inhibitory state
267 [34,35]. Several studies have suggested that the generation of burst firing mediated by
268 T-VGCC activation in certain regions is highly dependent on membrane potential [35,36],
269 and the NMDA receptor plays a critical role in regulating burst firing [26]. Glutamate is a
270 common excitatory neurotransmitter and its concentration around neurons may affect
271 membrane potential [37]. We applied different glutamate receptor antagonists into

272 artificial cerebrospinal fluid (ACSF) during whole-cell recordings of burst firing
273 neurons. Consistent with previous studies [26], our results indicated that blockade of
274 NMDA receptors, but not AMPA receptors, significantly inhibited burst firing and
275 caused membrane hyperpolarization, which made it more difficult to reach the
276 T-VGCC threshold (Extended Data Fig. 5).
277
278 **Knockdown of Cav3.1 in dmVMH decreased burst firing and ameliorated chronic**
279 **stress response**
280 Given the important role of Cav 3.1 in mediating burst firing in the dmVMH, we next
281 tested whether down-regulation of Cav 3.1 expression in the dmVMH was sufficient to
282 ameliorate anxiety-like behavior and energy metabolic changes induced by chronic
283 stress. We developed a lentivirus-mediated RNAi method to interfere with expression
284 of Cav3.1 in the dmVMH under chronic stress, with the shRNA-expressing vector
285 injected into the dmVMH bilaterally prior to chronic-stress exposure (Fig. 5a). To test
286 the efficacy of shRNA-mediated Cav3.1 silencing, we used immunofluorescence to
287 confirm the efficient knockdown of Cav3.1 in the dmVMH of stressed mice (Fig. 5b).
288 The effects of Cav3.1 knockdown on burst firing were tested using whole-cell
289 recording on brain slices obtained from Cav 3.1 knockdown mice. Results showed that
290 7 out of 17 dmVMH neurons from stressed mice displayed evoked burst firing, whereas
291 only 2 out of 13 dmVMH neurons succeeded after Cav3.1 knockdown (Fig. 5b),
292 suggesting burst firing inhibition induced by RNAi of Cav3.1.

293 To investigate phenotypic changes in Cav3.1 knockdown mice, we carried out
294 behavioral and energy metabolic tests after viral expression of shRNA of Cav3.1 for
295 4–5 weeks. Importantly, behavioral tests showed that Cav 3.1 knockdown significantly
296 increased residence time and entries into the central area of the open field and open arm
297 of the elevated plus-maze of stressed mice (Fig. 5c,d), suggesting that local knockdown
298 of Cav 3.1 in the dmVMH was sufficient to rescue stress-induced anxiety-like behavior.
299 For energy metabolic tests, we fasted all mice overnight and analyzed energy
300 expenditure using CLAMS. Data showed that Cav 3.1 silencing effectively rescued the
301 chronic stress-induced decrease in RER (Fig. 5f), as well as the reduction in food intake
302 (Fig. 5f) and energy expenditure (Fig. 5a and h). No obvious body weight differences
303 were observed among the control, stress, and RNAi groups (Fig. 5e).
304
305 Together with our optogenetic manipulation experiments, our results consistently
306 demonstrated that Cav 3.1 in the dmVMH was both sufficient and necessary to elicit
307 burst firing of dmVMH neurons. Furthermore, knockdown of Cav 3.1 in the dmVMH
308 ameliorated chronic stress-induced phenotypic abnormalities, including anxiety-like
309 behavior, lower RER, and decreased food intake.
310
311 **Discussion and conclusion**
312 Previous studies have indicated that the dmVMH is an important stress coping center to
313 balance aversive behavior and energy seeking [2] and may be a possible hub connecting
314 stress-induced emotion and energy expenditure. Here, we reported that chronic stress

315 induced burst firing enhancement in the dmVMH, which was critical for inducing
316 anxiety-like behavior and energy expenditure alteration in stressed mice. Bursting is an
317 important firing pattern in the central nervous system and is also important for specific
318 information transmission. Based on our data, we determined that dmVMH burst firing
319 neurons play an important role in connecting the emotional state of anxiety and energy
320 homeostasis, and that T-VGCC Cav 3.1 is essential for dmVMH burst firing and
321 contributes to chronic stress-induced behavior and energy expenditure changes (Figure
322 S6).
323

324 **dmVMH is responsive in chronic stress**

325 Chronic unpredictable stress is detrimental to both mental and physical health.
326 Responses to chronic stress can vary from emotional disorders, like anxiety and
327 depression, in the central nervous system to disturbed metabolism and energy
328 homeostasis in peripheral organs [3-5]. However, how these physiological processes
329 integrate in the brain and the underlying neural mechanisms remain poorly understood.
330 The dmVMH is implicated in integrating information in the limbic system and in
331 maintaining energy balance [38]. Furthermore, SF-1 neurons in the dmVMH constitute a
332 nutritionally sensitive switch, which modulates the competing motivations of feeding
333 and avoidance of environments full of acute stress [2]. Given the important role of the
334 dmVMH in balancing acute stress inputs and food-seeking, the effects of persistent
335 unpredictable stress on the function of dmVMH neurons require further research.

336

337 In the current study, the dmVMH was found to be involved in integrating chronic stress
338 inputs to regulate anxiety-like behavior and energy expenditure. We established an
339 unpredictable and persistent stress mouse model and characterized the model with
340 multiple energy metabolic, electrophysiological, and behavioral approaches.
341 Consistent with previous reports [3], we found that unpredictable persistent stress
342 induced aversive behavior, decreased food intake, and shifted the RER toward fat
343 oxidation, without obvious effects on body weight. Furthermore, *in vivo*
344 electrophysiology demonstrated that the power density of the theta band of local field
345 potential was higher in the stress group than in the control group. To dissect the
346 alteration in dmVMH neuronal activity under chronic stress conditions, we studied the
347 electrophysiology of dmVMH neurons. Based on differences in electrical activity, we
348 classified the dmVMH neurons into three subtypes: i.e., silent, tonic-firing, and
349 bursting. By comparing these subtypes in the control and stress groups, we found an
350 enhancement of burst firing in the dmVMH after chronic stress, including increased
351 percentage of burst firing neurons, enhanced LFP, and decreased ISI of bursts. Using
352 patch clamp recordings, our data demonstrated that chronic stressors indeed induced
353 obvious electrophysiological changes in dmVMH neurons at the cellular level, further
354 supporting the important role of the dmVMH in chronic stress.

355

356 **Burst firing of dmVMH is critical for chronic stress response**

357 Action potentials that arrive in bursts provide more precise information than action
358 potentials that arrive singly and further enhance the efficacy of neuromodulator release,
359 thus revealing the special role of bursts in information transmission and processing [30].
360 Many previous studies have indicated that burst firing of specific neuronal
361 subpopulations is critical for performing specific functions. In the hippocampus, a
362 single burst can produce long-term synaptic modifications [39]. In the hypothalamus,
363 burst firing is found in several regions, including the preoptic area and VMH [40]. In the
364 lateral habenula, bursting activity depends on the NMDA receptor and T-VGCC; and
365 most importantly, can drive behavioral aversion and depression-like symptoms [26]. To
366 date, however, no specific study has reported on the functions of dmVMH burst firing
367 under chronic stress. Here, we performed electrophysiological and gene expression
368 studies and demonstrated that burst firing neurons in the dmVMH are actively
369 involved in chronic stress response, and the ISI of burst firing was significantly
370 correlated with the anxiety-like behavior in anxious mice after chronic stress.
371
372 To mimic burst firing *in vivo*, we applied optogenetic inhibition with an
373 NpHR-expressing AAV vector, as optogenetic inhibition on the lateral habenula or
374 hippocampal NpHR-expressing neurons can elicit burst firing in yellow light
375 illumination intervals [26,41]. However, burst firing in the dmVMH could not be elicited
376 under an illumination frequency greater than 0.2 Hz in our electrophysiological
377 studies, indicating regional specificity of T-VGCC activation kinetics. Importantly, we

378 applied wireless optogenetics to successfully achieve burst manipulation in mice
379 residing within a closed cage, followed by behavioral and energy metabolic analyses.
380 Our data indicated that optogenetic-elicited burst firing was sufficient to promote the
381 chronic stress-induced phenotypes described above. Taken together, these data show
382 that VMH burst firing is an important hub for integrating and interacting anxiety-like
383 emotional state and energy expenditure regulation.
384

385 **Mechanism of burst firing in dmVMH**

386 The mechanism underlying neuronal burst firing is complicated and could explain
387 specific functions in different brain regions. Previous studies have reported that
388 various modulatory substances can promote depolarization of membranes and evoke
389 burst firing of neurons. Oxytocin binds to its receptor in CA2 region and can activate
390 the G protein-coupled pathway, and thus induce activation of several spike channels
391 and closure of KCNQ potassium channels [39]. Among the various mechanisms
392 underlying burst initiation, activation of a low-threshold ion channel can induce burst
393 firing in diverse brain regions [26,31]. Typically, low-threshold T-VGCC is widely
394 expressed in the central nervous system and can be activated by stimuli near the RMP
395 to elicit burst firing. Molecular cloning has revealed three isoforms of T-type channel
396 genes: i.e., Cav3.1, Cav3.2, and Cav3.3, which make distinct contributions to cellular
397 electrical properties [31,32,42]. Selective expression of Cav3.1 is sufficient to generate a
398 strong rebound burst in deep cerebellar nuclear neurons, whereas expression of

399 Cav3.2 or Cav3.3 alone does not generate a rebound discharge under normal
400 conditions [31]. Several studies have demonstrated that substitution of Cav3.1 or Cav3.2
401 for the native channel in model thalamic relay neurons causes elimination of
402 high-frequency bursts, further confirming the role of Cav3.1 in burst firing [32,42].
403
404 Here, we identified the existence of Cav3.1, Cav3.2, and Cav3.3 in the dmVMH
405 region. Cav3.1 and Cav3.2 displayed high expression in the dmVMH, whereas Cav3.3
406 showed lower expression, consistent with previous study [40]. The T-VGCC antagonist
407 mibefradil blocked burst firing of dmVMH neurons, thus suggesting the existence of
408 T-VGCC-mediated burst firing in the dmVMH. Furthermore, combined analysis of
409 electrophysiological classification and single-cell qRT-PCR, we found that Cav3.1
410 expression increased under chronic stress, which contributed to the enhancement of
411 burst firing in the dmVMH. Furthermore, Cav3.1 demonstrated greater contribution to
412 stress-induced enhancement of bursting in the dmVMH than the other isoforms.
413
414 We further investigated the necessity of Cav3.1 in chronic stress-induced anxiety-like
415 behavior and energy metabolic disorders. We found that microinjection of mibefradil
416 ameliorated anxiety-like behavior. Using RNAi methods, the expression of Cav3.1 in
417 the dmVMH was specifically knocked down, resulting in the significant inhibition of
418 neuronal bursting activity. Behavioral and energy expenditure experiments further
419 demonstrated that the chronic stress responses described above were partially rescued.

420 Thus, our findings consistently demonstrated that Cav3.1 may be a potential drug
421 target for the treatment of anxiety and related energy metabolic disorders.
422
423 The current study has several limitations. Firstly, we focused on exploring neuronal
424 activity changes in the dmVMH after chronic stress. As such, further research should
425 focus on identifying the mechanism regulating Cav3.1 expression in the dmVMH,
426 especially the receptors regulating Cav3.1 expression. Several factors might contribute
427 to the increased percentage of burst firing neurons after stress, including stress-induced
428 hormones or feeding-related peptides [24]. Previous studies have reported that estrogen
429 can regulate the expression and function of T-VGCC in vlVMH neurons, but not
430 dmVMH neurons, through estrogen receptors [40]. However, the mechanism underlying
431 Cav3.1 expression influenced by hormones or neuropeptides after chronic stress needs
432 further study.
433
434 Secondly, GABAergic neural circuits and astrocytes have been found in the VMH and
435 are implicated in regulating energy expenditure [43,44], but their specific contributions to
436 bursting activity need to be further investigated. We demonstrated that glutamate
437 receptors (especially NMDA receptors) affect the generation of burst firing; however,
438 whether synaptic glutamate uptake mediated by astrocytes affects burst firing requires
439 further exploration. Moreover, as the function of the T-VGCC is highly membrane
440 potential dependent, how upstream inputs integrate with the surrounding

441 microenvironment to affect membrane potential, and hence regulate burst firing,
442 needs to be further explored.
443
444 In summary, our study first identified bursting firing neurons in the dmVMH as a hub
445 regulating emotional state and energy metabolic disorders. We also identified Cav 3.1
446 as the crucial regulator of bursting firing of dmVMH neurons. The results of this
447 molecular and electrophysiological study should provide a more complete
448 understanding of the chronic stress-induced emotional malfunction and peripheral
449 metabolism disorders, and provides potential therapeutic targets for treating such
450 malfunctions.

451 **Competing interests**

452 The authors declare no competing interests.
453

454 **Acknowledgements**

455 This project was partly supported by the National Natural Science Foundation of
456 China (81471164, 31800881), Key Research Program of Frontier Sciences of Chinese
457 Academy of Sciences (QYZDB-SSW-SMC056), and Shenzhen Governmental Basic
458 Research Grant (JCYJ20170413164535041, JCYJ20180507182301299). We also
459 thank Z.B Xu and B.F Liu for their help in transgenic mice husbandry and
460 phenotyping. We are grateful to N.N Li and X.L Liu for the help in virus packaging.

461 **Author contributions**

462 F.Y. and H.-L.H. conceived the idea and designed the experiments. J.S. D.-S.G and

463 Y.-H.L performed all electrophysiological recordings, immunostaining, qRT-PCR and
464 behavioral experiments, S.-P.C. and X.-Y.Z. helped with patch clamp recording and
465 qRT-PCR, L.Z. helped with immunostaining and surgery, N.L. helped with the
466 RNAi construction, Q.X. helped with in vivo electrophysiological recording, F.Y. and
467 J.S. interpreted the results and wrote the manuscript with critical inputs from H.-L.H.
468 and L.-P.W..
469

470 **Methods**

471 **Animals**

472 All procedures were carried out in accordance with protocols approved by the Ethics
473 Committee of the Shenzhen Institutes of Advanced Technology, Chinese Academy of
474 Sciences. Male C57BL/6 mice (4–8 weeks old) were purchased from the Guangdong
475 Medical Laboratory Animal Center (Guangzhou, China). The SF-1-Cre mice (stock no:
476 012462) were obtained from Jackson Laboratories (Bar Harbor, ME, USA). Mice were
477 housed at 22–25 °C on a circadian cycle of 12-hour light and 12-hour dark with
478 ad-libitum access to food and water.

479 **Chronic stress procedures**

480 All animals used in this study were male, and randomly assigned to either control or
481 stress groups for chronic stress study. The stress group was daily subjected to one
482 stressor which randomly chosen from following: (i) 10 mice squeezing in a relatively

483 small cage (15 cm×10 cm×4 cm) for two hours. (ii) wet bedding in home cage
484 overnight (200 ml water was added to moisten bedding). (iii) each mouse was tightly
485 restraint in a tube for two hours. The chronic stress protocol lasted for 28 consecutive
486 days. Mice in different stress groups received the same number of each stressor.
487 Control animals were subjected to no stressors.

488 **Behavioral tests**

489 *Elevated plus maze (EPM).* Exposure (5-min) to EPM was used to assess locomotor
490 activity and anxiety-related behaviors after chronic stress. The stress and control
491 groups (n = 18–20/group) were placed in the center of the plus maze facing an open arm
492 and behavior was recorded for the entire 5 min using an overhead-mounted camera.
493 Videos recorded during the EPM test were analyzed with ANY-maze software
494 (Stoelting Co., Wood Dale, USA) to acquire data on time spent in open and closed arms,
495 locomotor activity (total distance travelled in maze), and entries into the open arm.
496 Anxiety-related behavior is associated with less exploration in the open arm relative to
497 overall exploration of all arms.

498 *Open field test (OFT).* Open field exposure (10-min) was used to assess locomotor
499 activity and anxiety-related behaviors after chronic stress. Mice (n = 18–20/group)
500 were placed in the center of an open field and behavior was recorded for the entire 10
501 min. Videos were analyzed to acquire data on time spent in the center and corner areas,
502 total locomotor activity, and number of entries into the center area. Anxiety-related
503 behavior is associated with less exploration of the center area.

504 **CLAMS and energy expenditure**

505 To characterize metabolic changes caused by chronic stress or Cav 3.1 knockdown,
506 RER was measured by indirect calorimetry using a four-chamber open-circuit
507 calorimeter (Oxymax Series; Columbus Instruments, Columbus, OH, USA). Mice were
508 food deprived overnight, with body weight and chow in each cage weighed prior to the
509 experiment. During the experiment, mice were housed individually in specially built
510 Plexiglas cages (40 × 25 × 20 cm). Temperature was maintained at 22 °C with an
511 airflow of 0.5 per min. Food and water were available *ad libitum*. Mice were
512 subsequently monitored in the system for 24 h (whole light-dark cycle). Oxygen
513 consumption (VO2) and carbon dioxide production (VCO2) were measured every 10
514 min. The RER was calculated as a quotient of VCO2/VO2, with 1 representing 100%
515 carbohydrate oxidation and 0.7 representing 100% fat oxidation. Energy expenditure
516 (kcal heat produced) was calculated as calorific value (CV) × VO2, where CV is 3.815
517 + 1.232 × RER [3]. Metabolic data collected from the 24-h monitoring period were
518 averaged for energy expenditure and RER. After the experiment, chow in each cage
519 was weighed to calculate food intake.

520 **Slice preparation**

521 Mice were deeply anesthetized with isoflurane and decapitated rapidly. Brains were
522 then removed and transferred to chilled cutting solution within 3 min. Cutting solution
523 contained (in mM): choline chloride 110; KCl 2.5; Na-pyruvate 0.6; $MgCl_2$ 7.0; $CaCl_2$

524 0.5; $NaH_2PO_4$ 1.3; $NaHCO_3$ 25; glucose 20 (pH 7.4). The chilled cutting solution was
525 bubbled with carbogen (95% $O_2$ and 5% $CO_2$) for at least 30 min before use. Coronal
526 slices (250–300 mm thick) were prepared on a vibratome (Series 1000, Warner
527 Instruments, Berlin, Germany), and incubated in artificial cerebrospinal fluid (ACSF)
528 containing (in mM): NaCl 125; KCl 2.5; Na-pyruvate 0.6; $MgCl_2$ 1.3; $CaCl_2$ 2.0;
529 $NaH_2PO_4$ 1.3; $NaHCO_3$ 25; glucose 10 (pH 7.4) bubbled with carbogen at 34 °C for 30
530 min. After incubation, all slices were equilibrated in ACSF at room temperature
531 (24–26 °C) for at least 40 min. Single slices were placed on the recording chamber
532 perfused with ACSF bubbled with carbogen at room temperature. Unless stated
533 otherwise, drugs were applied with perfused ACSF.

534 **Electrophysiology**

535 Whole-cell patch clamp recording was performed on VMH neurons. The dmVMH was
536 identified based on landmarks (third ventricle). Recordings were obtained with
537 multi-clamp 700B amplifiers (Molecular Devices, San Jose, USA) under visual
538 guidance using a Nikon FN1 microscope (Tokyo, Japan). Electrophysiological data
539 were acquired and analyzed using pClamp 10 software (Molecular Devices, San Jose,
540 USA ). Whole-cell recordings were performed with borosilicate glass electrodes (0.69
541 mm OD, 5–7 MΩ) with internal solution containing (in mM): K-gluconate 135.0; KCl
542 4.0; NaCl 2.0; HEPES 10; EGTA 4.0; Mg-ATP 4.0; Na-GTP 5.0. Osmolality was
543 adjusted to 290–310 mOsm $kg^{-1}$ with sucrose and pH was adjusted to 7.4 with KOH.
544

545 After forming a high-resistance seal (GΩ), the cell was held in current-clamp mode for
546 7–10 min until access resistance stabilized. Resting membrane potential (RMP) was
547 assessed at the beginning of the recording period after stabilization of access resistance,
548 and periodically monitored throughout the recording by momentarily relieving the
549 direct current injection. To elucidate differences among neurons, 800-ms current
550 injections (-100 to 100 pA in 10 pA increments; 5 s interstimulus interval) were applied,
551 and the number of action potentials evoked by each current injection, input resistance,
552 and half-width of action potentials were determined.

553 **Drugs and reagents**

554 All chemicals included in ACSF prescription were purchased from Sigma-Aldrich
555 (Merck KGaA, Darmstadt, Germany). Mibefradil (40 μM) were purchased from Tocris
556 (Bio-Techne, Minneapolis, USA) and used for electrophysiology and microinjection.
557 NBQX (1,2,3,4-tetrahydro-6-nitro-2,3-dioxo- benzo[f]quinoxaline-7-sulfonamide, 30
558 μM) and AP5 (2-amino-5-phosphono-pentanoic acid, 30 μM) were acquired from Med
559 Chem Express (MCE, Shanghai, China).

560 **Cell harvesting and single-cell Quantitative real-time polymerase chain reaction**
561 **(qRT-PCR)**

562 Single Cell-to-CT™ Kits (Thermo Fisher, USA) were used to perform single-cell
563 qRT-PCR. After recording, single cells were collected and lysed to acquire total RNA.
564 A Mastercycler 5333 PCR thermal cycler (Eppendorf, Germany) was used to perform

565 reverse transcription and pre-amplification. TaqMan gene expression assay was used to
566 assay each gene. Gene expression levels were normalized to the expression of
567 housekeeping gene *Rn18s*. All protocols were performed according to the
568 manufacturer's instructions. qRT-PCR was performed with a Light cycler 480 (Roche,
569 Switzerland).

570 **Tissue collection and qRT-PCR**

571 To acquire dmVMH tissue, mice were first anesthetized with isoflurane. After bathing
572 in cold 1% diethyl pyrocarbonate (DEPC) phosphate-buffered saline (PBS) solution,
573 brains were acute cut on a vibratome. VMH tissues were dissected microscopically
574 from those sections, and quickly transferred to TRIzol reagent. The manufacturer's
575 standard protocols for RNA extraction (TransGene, China) and synthesis (TOYOBO,
576 Japan) were followed. Primers used for qRT-PCR included: Cav 3.1 (5'-TGG
577 CCTTCTTCGTCCTGAAC-3' and 5'-TTCTCCAGCCTCTTTAGTCGC-3'). Cav 3.2
578 (5'-CGGCCCTACT ACGCAGACTA-3' and 5'-TTAAGGGCCTCGTCCAGAGA-3'),
579 Cav 3.3 (5'-CTGCTATTCTCCAGCCCAGG-3' and 5'-AGCTGCACCTCTTG
580 CTTGT-3'). Expression of these gene was normalized to the expression of
581 housekeeping gene β-Actin (*Act-b*).

582 ***In vivo* electrophysiology**

583 Mice were implanted with two nickel-chromium wires (25-μm diameter; AM Systems,
584 Sequim, USA) targeting the dmVMH, connector was bind to wires and fixed on skull
585 with dental cement. After total recovery from surgery, mice were returned to the

586 recording sessions. Neuronal activity was collected using a Plexon Multichannel
587 Acquisition Processor system (Plexon, Dallas, USA). Local field potentials (digitized
588 at 1 kHz sampling rate, low-pass filtered up to 250 Hz) were recorded simultaneously
589 for 90 min with a gain of 5 000×. After the recording sessions, mice were anesthetized
590 by pentobarbital sodium and perfused intracardially. The electrode recording position
591 was marked by histological staining.

592 **Stereotaxic surgery and viral injection**

593 For all stereotaxic surgery, 12–16-week-old mice were anesthetized by pentobarbital
594 sodium (0.3% in saline, 1 ml/100 g, intraperitoneally) and placed in a stereotaxic
595 apparatus for surgery. Stereotaxic surgical procedures were performed using standard
596 protocols. To target the dmVMH, bilateral brain injection coordinates relative to
597 bregma were chosen (AP, -1.58 mm; ML, ±0.3 mm; DV, -5.5 mm). Unless stated
598 otherwise, 0.4 μL of viral vector was injected into the VMH at a rate of 0.1 μL/min
599 using a 10-μL Hamilton syringe and a syringe infusion pump (World Precision
600 Instruments, USA).

601

602 For RNAi knockdown study, Cav3.1-shRNA (U6-shRNA-EF1a-copGFP-PGK-Puro)
603 was injected into the VMH with lenti-viral vector. Mice were housed for four weeks
604 following injection for viral expression. Anxiety-like behavior and metabolic tests were
605 performed at the end of the paradigm. To assess the knockdown effectiveness of Cav
606 3.1 shRNA, mice were perfused with 4% paraformaldehyde (PFA) and brain tissues

607 were removed for immunostaining analysis after the final session.

608 For microinjection, a stainless-steel guide-cannula (0.6 mm outer diameter and 0.4 mm
609 inner diameter, RWD, Shenzhen, China) was implanted into the diencephalon to target
610 the VMH (AP, -1.58 mm; ML, ±0.3 mm; DV, -5.0 mm). The guide-cannula was fixed to
611 the skull using dental cement and three stainless steel screws. Each guide-cannula was
612 sealed with a stainless-steel wire for protection from obstruction. Before behavioral
613 testing, the stainless-steel wire was replaced with an injection cannula (0.5 mm deeper
614 than guide-cannula to break astrocyte aggregation), through which the drug dissolved
615 in saline (400 nl) was delivered at 100 nl/min into the VMH. After microinjection, mice
616 were rested for 30 min before tests.

617 **Wireless optogenetic manipulation**

618 To achieve wireless optogenetic manipulation of burst firing neurons, AAV9-DIO
619 -NpHR-mCherry was injected unilaterally into the VMH in the left hemisphere. Mice
620 were housed for four weeks following injection for viral expression before initiation of
621 experiments. A copper coil with a light emitting diode (LED) on the right side of the tip
622 (Inper, Hangzhou, China) was implanted into the brain of NpHR-expressing mice, with
623 the LED located 0.2 μm left of the dmVMH. The coil and indicator were fixed on the
624 surface of the skull bone with Vetbond Tissue Adhesive (3M, USA). Charging the coil
625 was achieved through antennas surrounding the cage. To initiate burst firing of
626 dmVMH neurons, 550-nm yellow light stimulation was performed at 0.1 Hz (2 s/pulse)
627 in the NpHR-mCherry group during the metabolic (one illumination trial/12 h, each

628 trial lasted for 2 h) and behavioral tests (OFT, 10 min; EPM, 5 min).

629 **Immunohistochemistry**

630 Mice were first anesthetized by chloral hydrate (10% in saline, 1 ml/100 g,
631 intraperitoneally), then perfused with 0.01 M PBS and 50 mL of 4% PFA transcardially.
632 Brains were dissected and post-fixed in 4% PFA overnight and then transferred to 30%
633 w/v sucrose solution for cryoprotection until sinking. Sections from the entire
634 anterior-posterior range of the VMH were stained using an antibody specific to Cav3.1
635 (1: 100, Alomone labs, Cat# ACC-021, RRID: AB_2039779), Cav3.2 (1: 100,
636 Alomone labs, Cat#ACC-025, RRID: AB_2039781), or Cav 3.3(1: 100, Alomone labs,
637 Cat# ACC-009, RRID: AB_2039783). Briefly, sections were washed, permeabilized in
638 0.1% Triton X-100/PBS for 15 min/three times, washed again, and blocked in 10%
639 normal goat serum (NGS) (w/v)/0.1% Triton X-100/PBS for 30 min. Primary antibody
640 was added, and sections were incubated overnight at 4 ℃. The following day, sections
641 were washed with 0.01 mM PBS, incubated with incubated with secondary antibody
642 (Alexa Fluor 594 Goat Anti-Rabbit, Cat#115-585-003, RRID: AB_2338059 or Alexa
643 Fluor 488 Goat Anti-Rabbit, Cat#111-547-003 RRID: AB_2338058) in 1% NGS/0.1%
644 Triton X-100/PBS for 1 h at room temperature, then washed, mounted, and cover
645 slipped with mounting medium containing DAPI.

646 **Statistical analysis**

647 Slice electrophysiological data were analyzed with pCLAMP (Molecular Device, San
648 Jose, CA, USA). *In vivo* electrophysiology data were analyzed with NeuroExplorer 5.0

649 (Plexon, Dallas, USA). All data were imported into Prism 7 (GraphPad Software, La
650 Jolla, CA, USA) and normality was assessed using D'Agostino-Pearson tests to verify
651 the appropriateness of the following statistical analyses. Unless stated otherwise, the
652 data are presented as means ± SEM. Statistical significance was determined using
653 two-tailed unpaired Student's *t*-tests when comparing two groups, paired Student's
654 *t*-test when comparing the effects of different treatments in the same group. When
655 multiple measures were compared between groups (e.g., current-frequency curves),
656 repeated measures two-way analysis of variance (ANOVA) with Bonferroni's test was
657 used. Differences were considered significant at $P < 0.05$.
658
659 To classify dmVMH neurons, unsupervised cluster analysis was performed with SPSS
660 v19 (Chicago, IL, USA) using squared Euclidean distances. The parameters for cluster
661 analysis were chosen based on their lack of linear correlation with each other. The
662 following electrophysiological parameters were included for analysis: onset time,
663 evoked firing rate, input resistance, and potential sag by H-current
664 (Hyperpolarization-activated current). Resting potential were excluded from the
665 parameters for cluster analysis because of their linear correlation with onset times. All
666 electrophysiological parameters were converted into standardized z-scores before
667 clustering.
668
669

670 **References**


671 1 Koolhaas, J. M. *et al.* Coping styles in animals: current status in behavior and
672 stress-physiology. *Neuroscience & Biobehavioral Reviews* **23**, 925-935,
673 doi:https://doi.org/10.1016/S0149-7634(99)00026-3 (1999).
674 2 Viskaitis, P. *et al.* Modulation of SF1 Neuron Activity Coordinately Regulates
675 Both Feeding Behavior and Associated Emotional States. *Cell Reports* **21**,
676 3559-3572, doi:https://doi.org/10.1016/j.celrep.2017.11.089 (2017).
677 3 Hardaway, J. A. *et al.* Central Amygdala Prepronociceptin-Expressing Neurons
678 Mediate Palatable Food Consumption and Reward. *Neuron* **102**, 1088,
679 doi:https://doi.org/10.1016/j.neuron.2019.04.036 (2019).
680 4 Gross, C. & Hen, R. The developmental origins of anxiety. *Nature Reviews*
681 *Neuroscience* **5**, 545-552, doi:10.1038/nrn1429 (2004).
682 5 Lupien, S. J., McEwen, B. S., Gunnar, M. R. & Heim, C. Effects of stress
683 throughout the lifespan on the brain, behaviour and cognition. *Nature*
684 *Reviews Neuroscience* **10**, 434-445, doi:10.1038/nrn2639 (2009).
685 6 Furay, A. R., Bruestle, A. E. & Herman, J. P. The role of the forebrain
686 glucocorticoid receptor in acute and chronic stress. *Endocrinology* **149**,
687 5482-5490, doi:10.1210/en.2008-0642 (2008).
688 7 Isingrini, E. *et al.* Resilience to chronic stress is mediated by noradrenergic
689 regulation of dopamine neurons. *Nature Neuroscience* **19**, 560-563,
690 doi:10.1038/nn.4245 (2016).
691 8 Kuperman, Y. *et al.* Perifornical Urocortin-3 mediates the link between
692 stress-induced anxiety and energy homeostasis. *Proceedings of the National*
693 *Academy of Sciences of the United States of America* **107**, 8393-8398,
694 doi:10.1073/pnas.1003969107 (2010).
695 9 Cheung, C. C. *et al.* Sex-dependent changes in metabolism and behavior, as
696 well as reduced anxiety after eliminating ventromedial hypothalamus
697 excitatory output. *Molecular metabolism* **4**, 857-866,
698 doi:10.1016/j.molmet.2015.09.001 (2015).
699 10 Guo, M. *et al.* Role of the adipose PPARγ-adiponectin axis in susceptibility to
700 stress and depression/anxiety-related behaviors. *Molecular psychiatry* **22**,
701 1056-1068, doi:10.1038/mp.2016.225 (2017).
702 11 Grayson, B. E., Seeley, R. J. & Sandoval, D. A. Wired on sugar: the role of the
703 CNS in the regulation of glucose homeostasis. *Nature reviews. Neuroscience*
704 **14**, 24-37, doi:10.1038/nrn3409 (2013).
705 12 Silva, B. A. *et al.* Independent hypothalamic circuits for social and predator
706 fear. *Nature Neuroscience* **16**, 1731-1733, doi:10.1038/nn.3573 (2013).
707 13 Wang, L., Chen, I. Z. & Lin, D. Collateral pathways from the ventromedial
708 hypothalamus mediate defensive behaviors. *Neuron* **85**, 1344-1358,
709 doi:10.1016/j.neuron.2014.12.025 (2015).
710 14 Coutinho, E. A. *et al.* Activation of SF1 Neurons in the Ventromedial

Hypothalamus by DREADD Technology Increases Insulin Sensitivity in Peripheral Tissues. *Diabetes* **66**, 2372-2386, doi:10.2337/db16-1344 (2017).

15 Yadav, V. K. *et al.* A serotonin-dependent mechanism explains the leptin regulation of bone mass, appetite, and energy expenditure. *Cell* **138**, 976-989, doi:10.1016/j.cell.2009.06.051 (2009).

16 McClellan, K. M., Parker, K. L. & Tobet, S. Development of the ventromedial nucleus of the hypothalamus. *Frontiers in Neuroendocrinology* **27**, 193-209, doi:https://doi.org/10.1016/j.yfrne.2006.02.002 (2006).

17 Anderson, D. J. Circuit modules linking internal states and social behaviour in flies and mice. *Nature Reviews Neuroscience* **17**, 692, doi:10.1038/nrn.2016.125 (2016).

18 Hashikawa, K. *et al.* Esr1+ cells in the ventromedial hypothalamus control female aggression. *Nat Neurosci* **20**, 1580-1590, doi:10.1038/nn.4644 (2017).

19 Kim, D. W. *et al.* Multimodal Analysis of Cell Types in a Hypothalamic Node Controlling Social Behavior. *Cell* **179**, 713-728.e717, doi:10.1016/j.cell.2019.09.020 (2019).

20 Wang, C., Bomberg, E., Billington, C. J., Levine, A. S. & Kotz, C. M. Brain-derived neurotrophic factor (BDNF) in the hypothalamic ventromedial nucleus increases energy expenditure. *Brain research* **1336**, 66-77, doi:https://doi.org/10.1016/j.brainres.2010.04.013 (2010).

21 Klöckener, T. *et al.* High-fat feeding promotes obesity via insulin receptor/PI3K-dependent inhibition of SF-1 VMH neurons. *Nature Neuroscience* **14**, 911-918, doi:10.1038/nn.2847 (2011).

22 Kunwar, P. S. *et al.* Ventromedial hypothalamic neurons control a defensive emotion state. *eLife* **4**, doi:10.7554/eLife.06633 (2015).

23 Iigaya, K., Okazaki, S., Minoura, Y. & Onimaru, H. Interaction between novel oscillation within the ventromedial hypothalamus and the sympathetic nervous system. *Neuroscience* **343**, 213-221, doi:10.1016/j.neuroscience.2016.11.048 (2017).

24 Iigaya, K., Minoura, Y., Onimaru, H., Kotani, S. & Izumizaki, M. Effects of Feeding-Related Peptides on Neuronal Oscillation in the Ventromedial Hypothalamus. *J Clin Med* **8**, 292, doi:10.3390/jcm8030292 (2019).

25 Wang, G. *et al.* CaV3.2 calcium channels control NMDA receptor-mediated transmission: a new mechanism for absence epilepsy. *Genes & development* **29**, 1535-1551, doi:10.1101/gad.260869.115 (2015).

26 Cain, S. M. *et al.* CaV3.2 drives sustained burst-firing, which is critical for absence seizure propagation in reticular thalamic neurons. *Epilepsia* **59**, 778-791, doi:10.1111/epi.14018 (2018).

27 Yuan, Y. *et al.* Reward Inhibits Paraventricular CRH Neurons to Relieve Stress. *Current Biology* **29**, 1243-1251.e1244, doi:10.1016/j.cub.2019.02.048 (2019).

28 Yang, Y. *et al.* Ketamine blocks bursting in the lateral habenula to rapidly relieve depression. *Nature* **554**, 317-322, doi:10.1038/nature25509 (2018).

29 Lee, S., Lee, C., Woo, C., Kang, S. J. & Shin, K. S. Chronic social defeat stress-induced enhancement of T-type calcium channels increases burst-firing neurons in the ventral subiculum. *Biochemical and biophysical research communications* **508**, 1182-1187, doi:10.1016/j.bbrc.2018.12.073 (2019).

30 Lisman, J. E. Bursts as a unit of neural information: making unreliable synapses reliable. *Trends Neurosci* **20**, 38-43, doi:10.1016/s0166-2236(96)10070-9 (1997).

31 Molineux, M. L. *et al.* Specific T-type calcium channel isoforms are associated with distinct burst phenotypes in deep cerebellar nuclear neurons. *Proceedings of the National Academy of Sciences of the United States of America* **103**, 5555-5560, doi:10.1073/pnas.0601261103 (2006).

32 McRory, J. E. *et al.* Molecular and functional characterization of a family of rat brain T-type calcium channels. *The Journal of biological chemistry* **276**, 3999-4011, doi:10.1074/jbc.M008215200 (2001).

33 Nelson, M. T. *et al.* Molecular mechanisms of subtype-specific inhibition of neuronal T-type calcium channels by ascorbate. *The Journal of neuroscience : the official journal of the Society for Neuroscience* **27**, 12577-12583, doi:10.1523/jneurosci.2206-07.2007 (2007).

34 Sherman, S. M. Tonic and burst firing: dual modes of thalamocortical relay. *Trends in Neurosciences* **24**, 0-126 (2001).

35 Cui, Y. *et al.* Astroglial Kir4.1 in the lateral habenula drives neuronal bursts in depression. *Nature* **554**, 323-327, doi:10.1038/nature25752 (2018).

36 Cain, S. M. *et al.* GABAB receptors suppress burst-firing in reticular thalamic neurons. *Channels (Austin, Tex.)* **11**, 574-586, doi:10.1080/19336950.2017.1358836 (2017).

37 Matott, M. P., Kline, D. D. & Hasser, E. M. Glial EAAT2 regulation of extracellular nTS glutamate critically controls neuronal activity and cardiorespiratory reflexes. *The Journal of physiology* **595**, 6045-6063, doi:10.1113/jp274620 (2017).

38 Steffens, A. B., Scheurink, A. J. W., Luiten, P. G. M. & Bohus, B. Hypothalamic food intake regulating areas are involved in the homeostasis of blood glucose and plasma FFA levels. *Physiology & Behavior* **44**, 581-589, doi:https://doi.org/10.1016/0031-9384(88)90322-8 (1988).

39 Tirko, N. N. *et al.* Oxytocin Transforms Firing Mode of CA2 Hippocampal Neurons. *Neuron* **100**, 593-608.e593, doi:10.1016/j.neuron.2018.09.008 (2018).

40 Qiu, J. *et al.* Estrogen upregulates T-type calcium channels in the hypothalamus and pituitary. *The Journal of neuroscience : the official journal of the Society for Neuroscience* **26**, 11072-11082, doi:10.1523/jneurosci.3229-06.2006 (2006).

41 Berglind, F. *et al.* Optogenetic inhibition of chemically induced hypersynchronized bursting in mice. *Neurobiology of Disease* **65**, 133-141,

795 doi:https://doi.org/10.1016/j.nbd.2014.01.015 (2014).
796 42 Cain, S. M. & Snutch, T. P. Contributions of T-type calcium channel isoforms to
797 neuronal firing. *Channels* **4**, 475-482, doi:10.4161/chan.4.6.14106 (2010).
798 43 Bouyakdan, K. *et al.* The gliotransmitter ACBP controls feeding and energy
799 homeostasis via the melanocortin system. *The Journal of clinical investigation*
800 **129**, 2417-2430, doi:10.1172/jci123454 (2019).
801 44 Chan, O. *et al.* Increased GABAergic Output in the Ventromedial
802 Hypothalamus Contributes to Impaired Hypoglycemic Counterregulation in
803 Diabetic Rats. *Diabetes* **60**, 1582-1589, doi:10.2337/db10-1579 (2011).

804

805

806 **Figure**

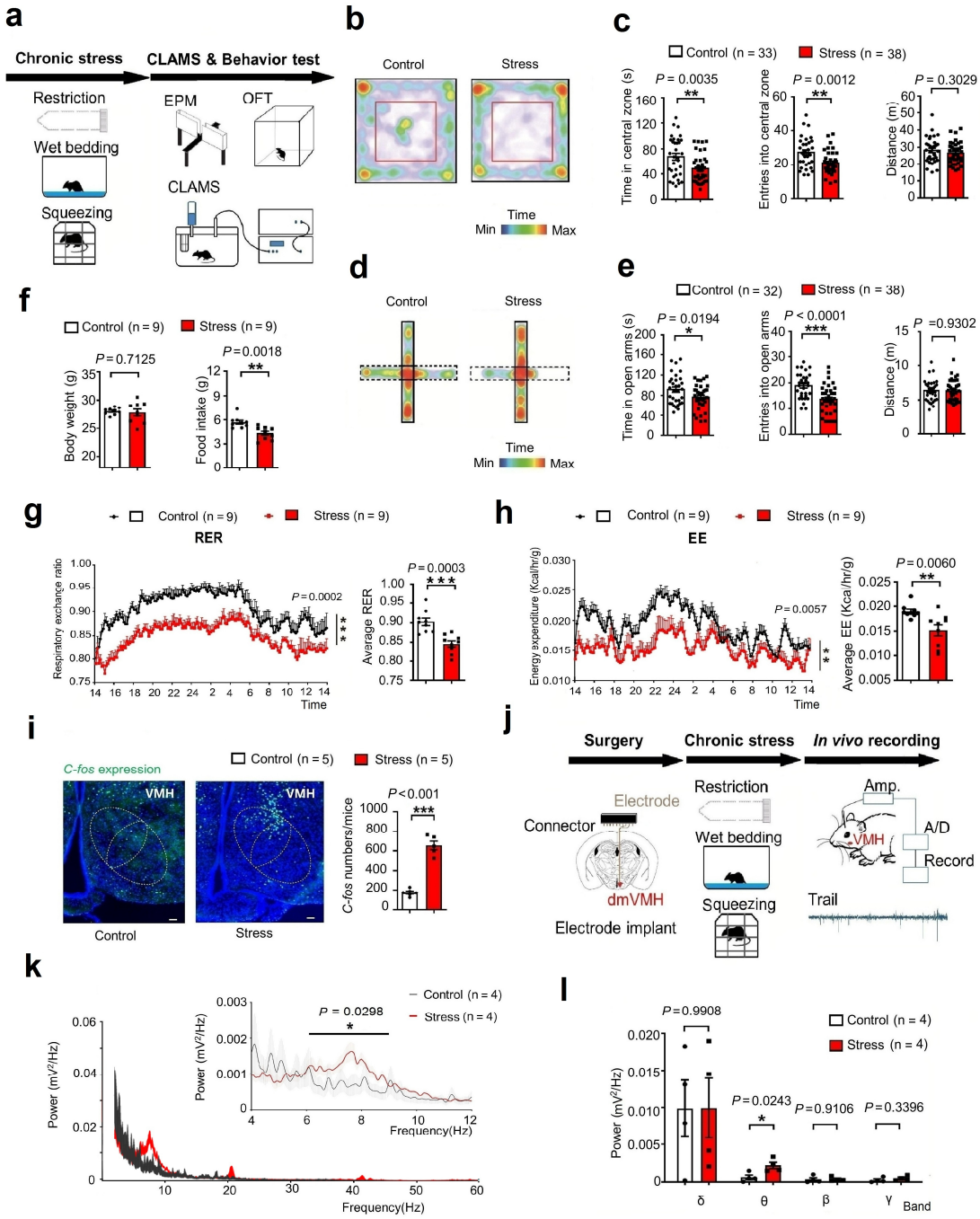


807

808 **Fig. 1| Chronically stressed mice exhibited anxiety-like behavior, altered**

809 **metabolism, and *in vivo* electrophysiological dmVMH activity.**

810 **(a)** Illustration of unpredictable chronic stress protocol and phenotype assessment, with

811 one stressor treatment randomly chosen per day, lasting for four weeks. **(b)** Residence

812 time in each site of open field (blue, less time; red, more time). **(c)** Behavioral analysis
813 of control (n = 33) and stress group mice (n = 38) in open field test showed significant
814 decrease in both time spent in central area (unpaired Student's *t*-test, $P = 0.0035$) and
815 entries into central area (unpaired Student's *t*-test, $P = 0.0012$), but no obvious change
816 in travelling distance (unpaired Student's *t*-test, $P = 0.3029$). **(d)** Residence time in each
817 site of elevated plus-maze (blue, less time; red, more time) of control and stress groups.
818 **(e)** Control (n = 32) and stress groups (n = 38) in elevated plus-maze showed significant
819 decrease in time spent in open arm (unpaired Student's *t*-test, $P = 0.0194$) and entries
820 into open arm (unpaired Student's *t*-test, $P < 0.0001$), but no obvious change in
821 locomotion (unpaired Student's *t*-test, $P = 0.9302$). **(f)** Body weight monitored after
822 chronic stress period showed no obvious change compared with naïve mice (n = 9 in
823 each group, unpaired Student's *t*-test, $P = 0.7125$), and 24-h food intake after overnight
824 fasting decreased in stress group (n = 9 in each group, unpaired Student's *t*-test, $P =$
825 $0.0018$) compared with control group (n = 9). **(g)** Average respiration exchange ratio
826 (RER) decreased in stress group compared with control group (unpaired student's *t*-test,
827 $P = 0.0003$, n = 9 mice in each group); RER curve shifted after chronic stress (two-way
828 ANOVA, $P = 0.0002$, $F(1, 16) = 21.95$). **(h)** Significant decreases in 24-h energy
829 expenditure (EE) curve and average EE were observed in stress group (two-way
830 ANOVA, $P = 0.0057$, $F(1, 16) = 20.2$; unpaired Student's *t*-test, $P = 0.0060$). **(i)**
831 Increased *c-fos* expression in dmVMH under chronic stress (unpaired Student's *t*-test, $P$
832 $< 0.001$, n = 5 mice in each group). **(j)** Schematic of electrode implantation and *in vivo*

833 electrophysiology recordings. **(k** and **l)** Power spectral density of local field potential

834 (LFP) in dmVMH after chronic stress, with significant power improvement observed in

835 theta band (two-way ANOVA, $P = 0.0298$, $F(1, 14) = 5.845$,; unpaired Student's *t*-test,

836 $P = 0.0243$, n = 4). Data are means ± SEM. * $P < 0.05$, ** $P < 0.01$, *** $P < 0.001$.

837 CLAMS, comprehensive laboratory animal monitoring system.

838

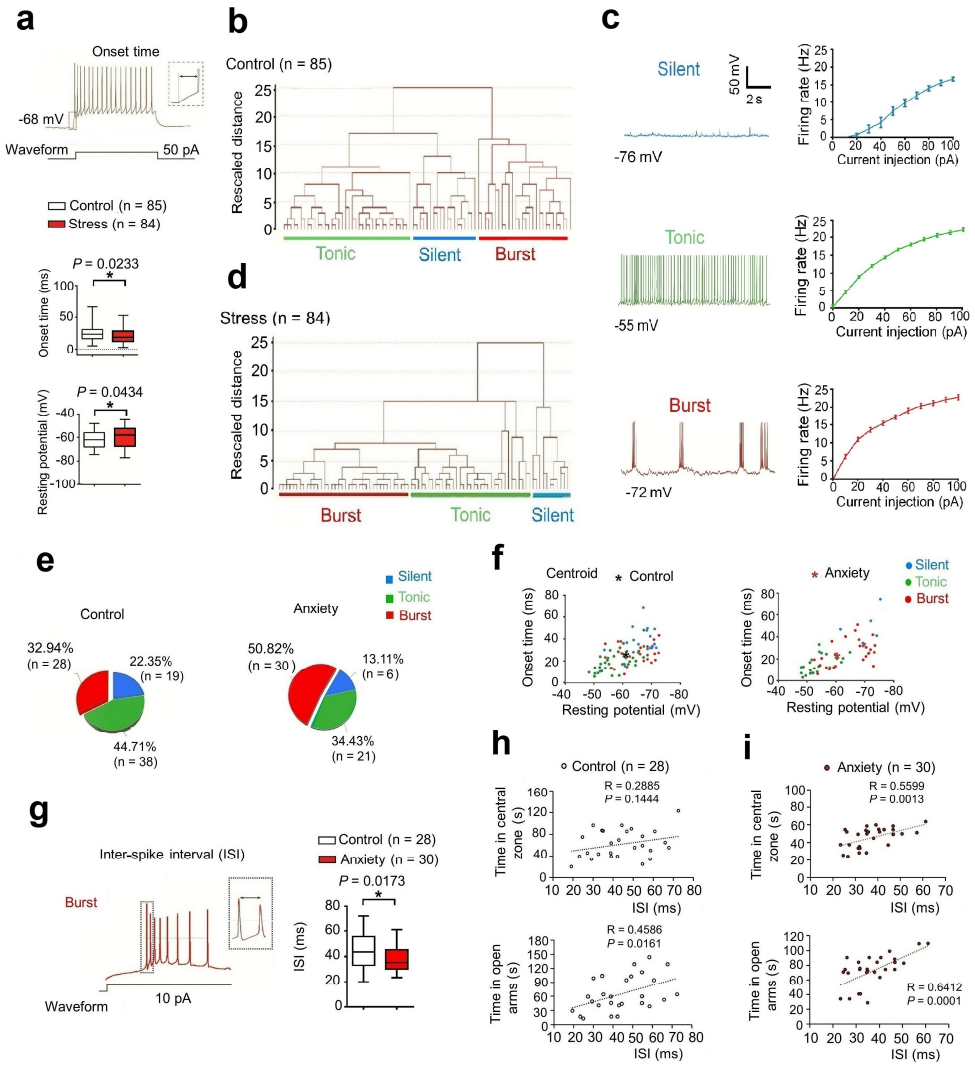


**Fig. 2| Chronic stress-induced enhancement of burst firing in dmVMH neurons.** **(a)** Increased average onset time (unpaired Student's *t*-test, $P = 0.0233$) and depolarized average resting membrane potential (RMP) (unpaired Student's *t*-test, $P = 0.0434$) in 84 dmVMH neurons from stressed mice compared with 85 neurons from wild-type mice. The box plotted at the median extending from the 25-75th percentile, and the whisker represents Min to Max distribution. **(b)** Cluster analysis of 85 dmVMH neurons from 35 normal mice. Dendrogram of cluster analysis shows that dmVMH neurons could be classified into three subtypes: i.e., silent, tonic-firing, and bursting. **(c)**

848 Electrophysiological properties of silent, tonic-firing, and bursting dmVMH neuronal
849 subtypes. left: whole-cell recording traces of three neuronal subtypes without current
850 injection; right: frequency-current curve of three subtypes at current injections of 0 to
851 100 pA and 10 pA/step. **(d)** Cluster analysis of 84 dmVMH neurons from 39 stressed
852 mice. Dendrogram of cluster analysis shows these dmVMH neurons can be classified
853 into three subtypes: i.e., silent (n = 13), tonic-firing (n = 35), and bursting (n = 38). See
854 also Figure S1 and S2. **(e)** Pie chart of percentages of neuronal dmVMH subtypes in
855 control group and stressed mice with obvious anxiety-like behavior (anxiety group). **(f)**
856 Distribution of 85 dmVMH neurons in control mice (left) and 57 dmVMH neurons in
857 anxiety group (right) using onset time-RMP coordinate system, with coordinate of
858 centroid (★) indicating average onset time and RMP. Blue, silent; Green, tonic-firing;
859 Red, bursting. Centroid coordinate was determined by average onset time and RMP.
860 Shift in centroid after chronic stress represents shorter average onset time and more
861 depolarized average RMP, caused by changes in proportion of three subtypes. **(g)**
862 Inter-spike interval (ISI) of bursts in dmVMH neurons of control and stressed mice.
863 Left, Example of burst firing and ISI; right, ISI of burst firing dmVMH neurons (n = 30)
864 in anxiety group decreased significantly compared with that in control group (n = 28,
865 unpaired Student's *t*-test, $P = 0.0099$). **(h)** ISI of dmVMH bursting neurons in control
866 group is slightly correlated with the residing time in open arms of EPM, but not with
867 the time spent in central area of open field (n = 28 cells from 21 mice). **(i)** ISI of
868 dmVMH bursting neurons in stressed mice which displayed obvious anxiety behavior

869 is significantly correlated with both the residing time in open arms and the time in

870 central area of open field (n = 30 cells from 20 mice). Data are means ± SEM * $P <$

871 0.05, ** $P < 0.01$.

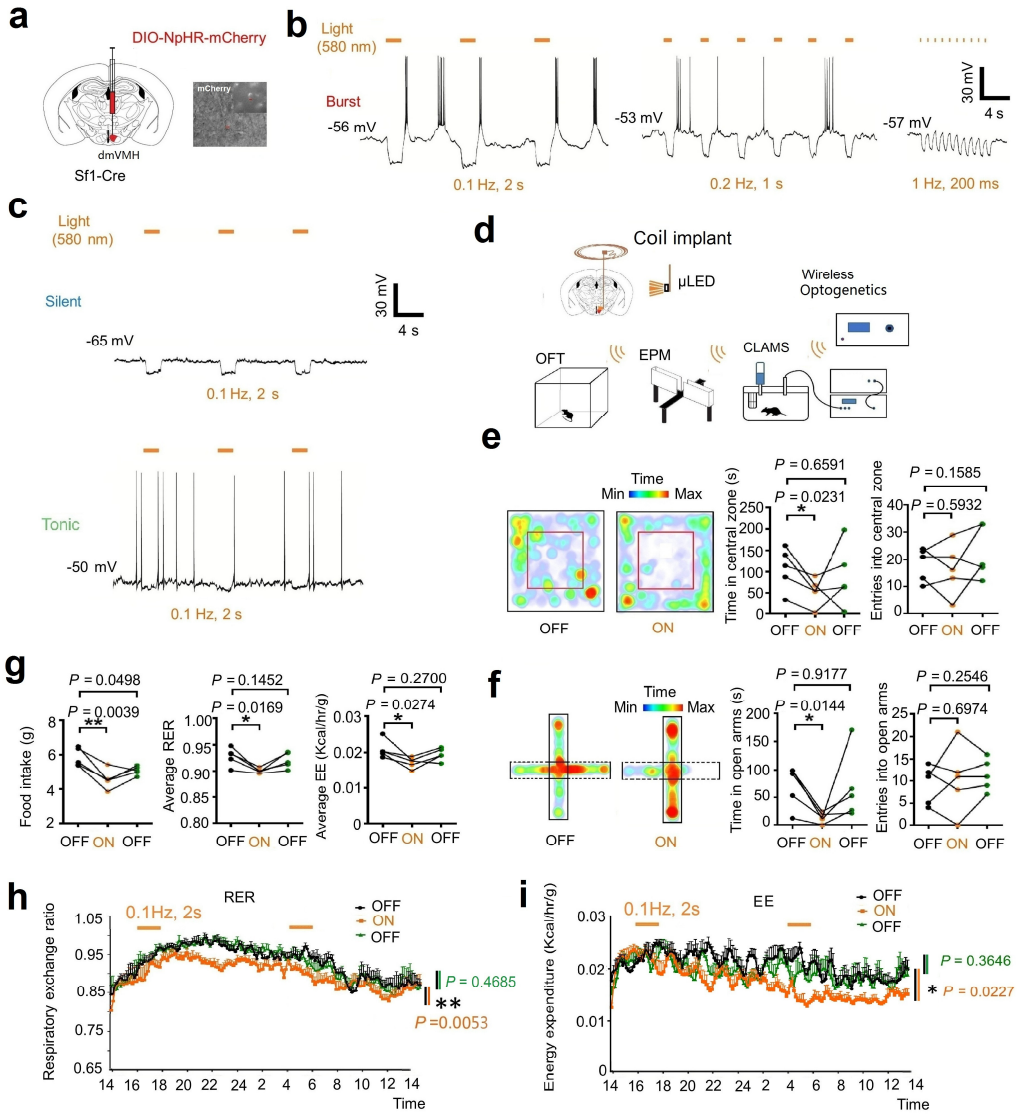


**Fig. 3| Optogenetic activation of burst firing neurons in dmVMH induced anxiety-like behavior and energy expenditure changes.**

**(a)** Schematic of dmVMH injection of NpHR AAV viral vector to induce burst firing *in vivo*. **(b)** Whole-cell recordings of yellow light-evoked burst firing in brain slices (yellow light: 590 nm, left: 0.1 Hz, 2 s; middle: 0.2 Hz, 1 s; right: 1 Hz, 200 ms), 0.1 Hz successfully induced activation of burst firing neurons. **(c)** 0.1 Hz and 2 s yellow light illumination exerted no significant influence on silent or tonic-firing dmVMH neurons. **(d)** Illustration of wireless optogenetic manipulation of dmVMH neurons and

881 behavioral analysis in free-moving mice. **(e)** Open field test before, during, and after
882 light illumination: residence time in central area decreased during 10-min yellow light
883 illumination (n = 5, paired Student's *t*-test, $P = 0.0237$), though no obvious changes
884 were observed in number of entries into central area (paired Student's *t*-test, $P =$
885 $0.5932$). **(f)** Elevated plus-maze test before, during, and after 5-min light illumination.
886 Residence time in open arms decreased during yellow light illumination (n = 5, paired
887 Student's *t*-test, $P = 0.0144$) and recovered after light-off; no obvious changes were
888 observed in number of entries into open arms (paired Student's *t*-test, $P = 0.6974$). **(g)**
889 Food intake and metabolism were monitored during optogenetic manipulation of
890 dmVMH neurons in free-moving mice. Food intake decreased during light stimulation
891 (paired Student's *t*-test, $P = 0.0039$, n = 5 mice in each group), also average RER
892 (paired Student's *t*-test, $P = 0.0169$) and EE (paired Student's *t*-test, $P = 0.0274$). **(h** and
893 **i)** RER and EE curve shifted (two-way ANOVA, RER: $P = 0.0053$, $F(1, 8) = 14.38$; EE:
894 $P = 0.0227$, $F(1, 8) = 7.7918$ ) when applying two yellow light stimulation trials (0.1 Hz,
895 2 s; for 2 h). Data are means ± SEM; * $P < 0.05$, ** $P < 0.01$.
896

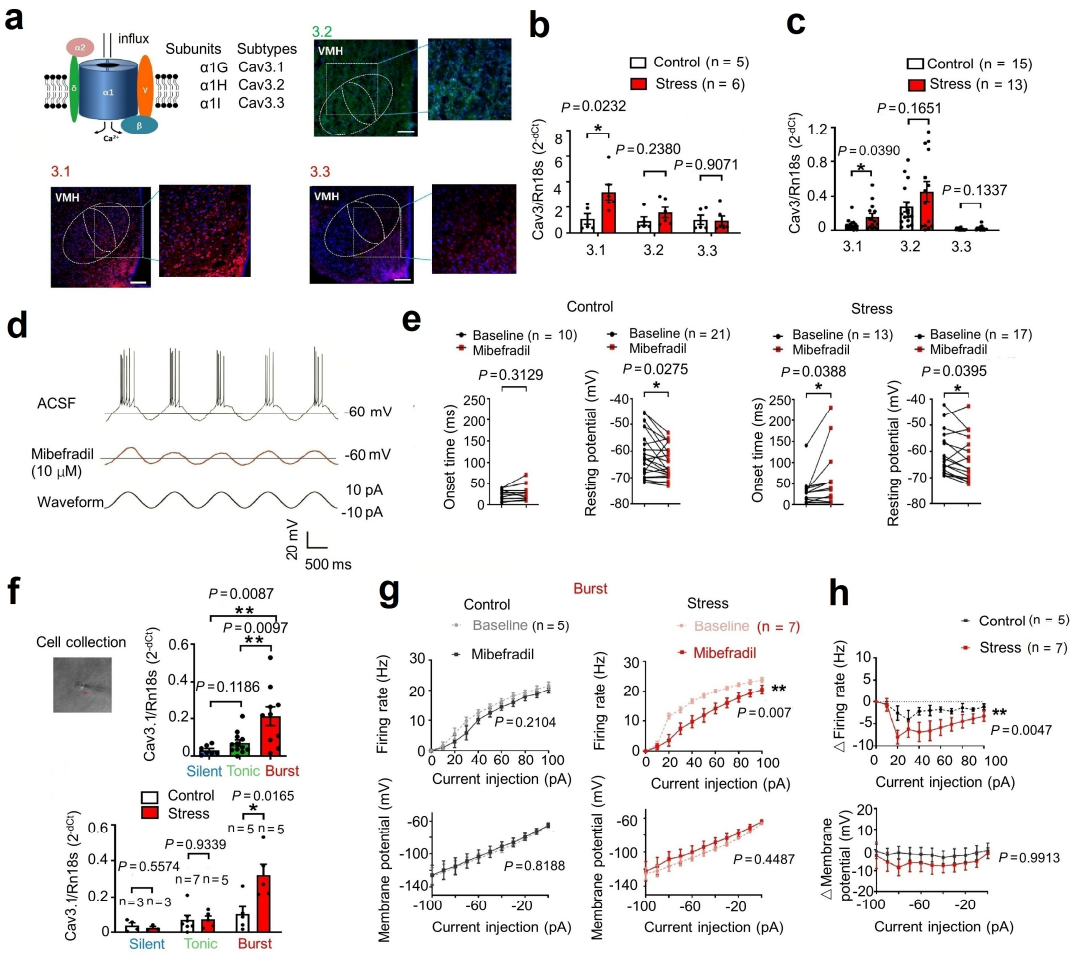


**Fig. 4| T-VGCC mediated enhancement of burst firing in dmVMH neurons under chronic stress.**

**(a)** Schematic of structure of T-VGCC located on cell membrane (left top). Representative immunofluorescence showing Cav 3.1 (left bottom), Cav 3.2 (right top), and Cav 3.3 (right bottom) expression in dmVMH, respectively, with stronger Cav3.1 expression observed. Scale bar is 200 μm. **(b)** Quantification of Cav 3.1, Cav 3.2, and Cav 3.3 expression in dmVMH tissue between control (n = 5 mice) and chronic stress groups (n = 6 mice). Expression of Cav 3.1 was significantly up-regulated under chronic stress conditions (unpaired Student's *t*-test, $P$ = 0.0232). **(c)** Single-cell qRT-PCR analysis of Cav 3.1, Cav 3.2, and Cav 3.3 expression in dmVMH neurons

908 between control (n = 16 cells) and chronic stress groups (n = 14 cells). Expression of
909 Cav 3.1 was significantly up-regulated under chronic stress conditions (unpaired
910 Student's *t*-test, $P = 0.0390$). **(d)** Evoked burst firing trace of dmVMH neurons without
911 and with T-VGCC antagonist (mibefradil, 10 μM), 10 pA current injection was given in
912 cosine waveform. **(e)** Effects of mibefradil on onset time and RMP of dmVMH neurons
913 from wild-type (n = 15) and chronic stress groups (n = 13). Significant differences were
914 observed in both onset time and RMP (paired Student's *t*-test, $P = 0.0388$ and $P =$
915 $0.0395$) in the stress group, whereas the control group demonstrated obvious changes in
916 RMP but not onset time (paired Student's *t*-test, $P = 0.0275$ and $P = 0.3125$). **(f)**
917 Single-cell qRT-PCR analysis of Cav 3.1 expression among three neuronal subtypes in
918 dmVMH. Upper: burst firing neurons (n = 11) showed higher Cav 3.1 expression than
919 other two subtypes (unpaired Student's *t*-test, $P = 0.0133$ compared with silent neurons
920 (n = 7), $P = 0.0139$ compared with tonic-firing neurons (n = 12)); bottom: Cav 3.1
921 expression in burst firing subtype showed significant differences between control and
922 chronic-stress groups (unpaired Student's *t*-test, silent: control, n = 3, stress, n = 3, $P =$
923 $0.5574$; tonic-firing: control, n = 7, stress, n = 5, $P = 0.9339$; bursting: control, n = 5,
924 stress, n = 6, $P = 0.0165$). **(g)** Effects of mibefradil on suprathreshold and subthreshold
925 activity in dmVMH burst firing neurons in control (n = 5) and chronic stress groups (n =
926 7). Mibefradil inhibited T-VGCC and caused a right frequency-current curve shift
927 (two-way ANOVA, control, $P = 0.2140$, $F(1, 8) = 1.854$; stress, $P = 0.0077$, $F(1, 12) =$
928 $10.22$); lower, mibefradil application exerted no obvious influence on current-voltage

929 curve of burst neurons (two-way ANOVA, control, $P$ = 0.8188, $F(1, 10)$ = 0.0573;

930 stress, $P$ = 0.4487, $F(1, 10)$ = 0.6218). **(h)** Obvious differences were observed in

931 suprathreshold activity (two-way ANOVA, $P$ = 0.0047, $F(1, 110)$ = 20.53), but not in

932 subthreshold (two-way ANOVA, $P$ = 0.9913, $F(1, 33)$ = 4.958) membrane potential of

933 dmVMH burst firing neurons between control (n = 5) and chronic stress groups (n = 7)

934 after application of mibefradil. Data are means ± SEM. * $P < 0.05$, ** $P < 0.01$.

935

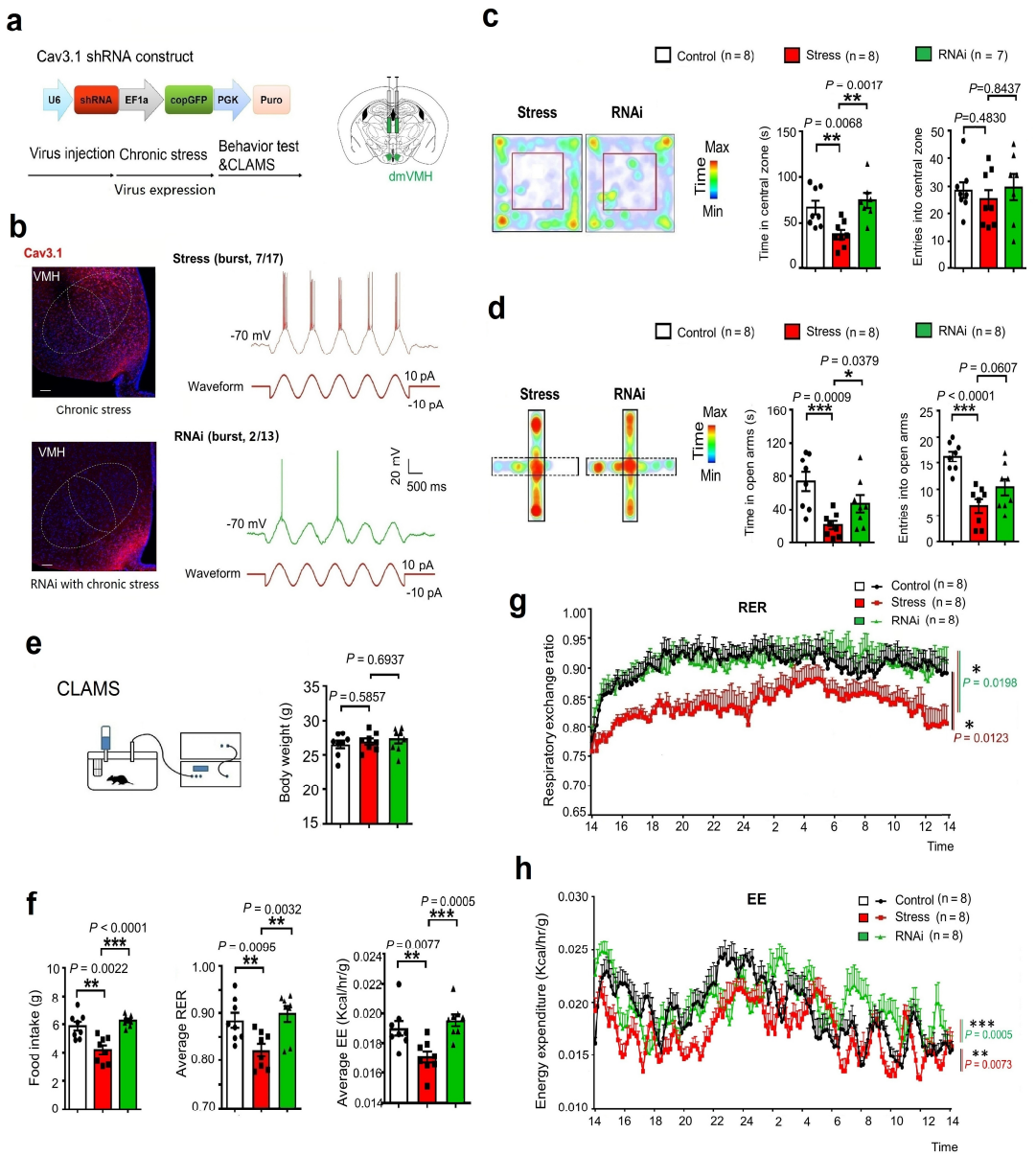


**Fig. 5| Knockdown of Cav3.1 in dmVMH decreased burst firing, and rescued anxiety-like behavior and metabolic alteration induced by chronic stress.**

**(a)** Schematic of Cav3.1 shRNA construct and injection of shRNA-expressing lenti-viral vector into dmVMH to interfere with Cav 3.1 expression. **(b)** Representative images of dmVMH Cav 3.1 immunostaining in chronic stress and RNAi (under chronic stress) animals (left). Proportion of burst firing neurons decreased in RNAi group (2/13, 15.38%) compared with stress group (7/17, 41.18%) (right). Scale bar is 100 μm. **(c)**

944 Time spent in central area and number of entries into central area of open field in
945 control, chronic stress, and RNAi groups. Residence time: control (n = 8) versus
946 chronic stress group (n = 8), $P = 0.0068$; chronic stress versus RNAi group (n = 7), $P =$
947 $0.0017$. Number of entries: control versus chronic stress group, $P = 0.4830$; chronic
948 stress versus RNAi group, $P = 0.8437$ (unpaired Student's *t*-test). **(d)** Time spent in
949 open arm and number of entries into open arm of elevated plus-maze in control, chronic
950 stress, and RNAi groups. Residence time: control versus chronic stress group, $P =$
951 $0.0009$; chronic stress versus RNAi group, $P = 0.0379$. Number of entries: control
952 versus chronic stress group, $P < 0.0001$; chronic stress versus RNAi group, $P = 0.0607$
953 (unpaired Student's *t*-test, 8 mice in each group). **(e)** No significant differences in
954 average body weights of control (n = 8), chronic stress (n = 8) and RNAi (n = 8) groups
955 were observed after four weeks of chronic stress (unpaired Student's *t*-test, control
956 versus stress group, $P = 0.5857$; chronic stress versus RNAi group, $P = 0.6937$). **(f)**
957 Food intake of mice in control, chronic stress, and RNAi groups: control versus chronic
958 stress group, $P = 0.0022$; chronic stress versus RNAi group, $P < 0.0001$ (unpaired
959 Student's *t*-test, 8 mice in each group). Average RER of control, chronic stress, and
960 RNAi groups (unpaired Student's *t*-test: control versus chronic stress group, $P = 0.0095$;
961 chronic stress versus RNAi group, $P = 0.0032$). Average EE of control, chronic stress,
962 and RNAi groups (unpaired Student's *t*-test: control versus chronic stress group, $P =$
963 $0.0077$; chronic stress versus RNAi group, $P = 0.0005$). **(g)** 24-h RER curve of control,
964 chronic stress, and RNAi groups (two-way ANOVA: control versus chronic stress

965 group, $P = 0.0123$, $F(1, 14) = 8.244$; chronic stress versus RNAi group, $P = 0.0198$, $F(1,$

966 $13) = 7.055$; 8 mice in each group). **(h)** 24-h EE curve of control, chronic stress, and

967 RNAi groups (two-way ANOVA: control versus chronic stress group, $P = 0.0005$, $F(1,$

968 $14) = 20.21$; chronic stress versus RNAi group, $P = 0.0073$, $F(1, 14) = 9.851$; 8 mice in

969 each group).Data are means ± SEM, * $P < 0.05$, ** $P < 0.01$, *** $P < 0.001$.

970

971 **Table 1. Electrophysiological properties of three dmVMH neuronal subtypes**

| | Silent (n = 19) | Tonic-firing (n = 38) | Bursting (n = 28) |
|---|---|---|---|
| Input resistance (MΩ) | 535.30 ± 21.83 | 661.72 ± 19.84 | 662.72 ± 24.21 |
| Onset Time (ms, 50 pA) | 37.17 ± 2.53 | 18.20 ± 1.28 | 25.84 ± 1.87 |
| RMP (mV) | -65.27 ± 1.08 | -57.50 ± 0.92 | -63.39 ± 1.07 |
| Overshoot by H-current (mv, -100 pA) | 7.26 ± 1.17 | 10.71 ± 0.94 | 12.01 ± 1.19 |
| Evoke firing rate (Hz, 100 pA) | 17.53 ± 0.60 | 21.76 ± 0.50 | 22.00 ± 0.73 |
| AHP (mV) | -12.38 ± 0.53 | -15.2 ± 0.50 | -14.26 ± 0.65 |
| Half width (ms) | 2.17 ± 0.08 | 2.00 ± 0.04 | 2.04 ± 0.05 |
| AP amplitude (mV) | 71.79 ± 1.88 | 73.29 ± 1.25 | 76.27 ± 1.28 |

972 Data are represented as mean ± SEM. RMP: resting membrane potential; H-current:

973 hyperpolarization-activated current; AHP: after-hyperpolarization potential; AP: action

974 potential.

975

976 **Supplemental Information**

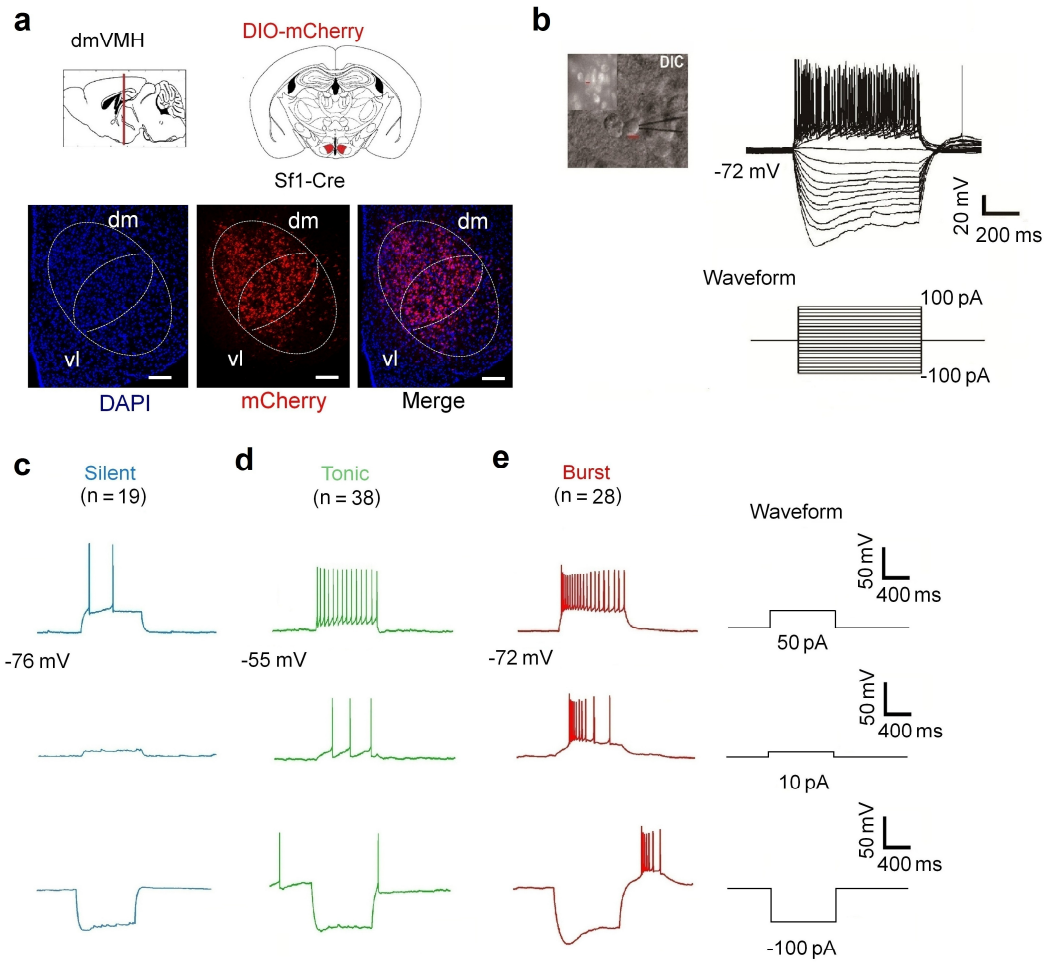


977

978 **Extended Data Fig. 1| Electrophysiological properties of dmVMH neurons**

979 **subtypes.** Related to Fig. 2.

980 (**a**) Schematic of location of dmVMH in coronal section slice of mouse brain, mCherry

981 was specifically expressed in SF-1 (specific dmVMH marker) neurons. Scale bar is 300

982 μm. **(b)** Whole-cell recording trace from a dmVMH neuron, with current injection of

983 -100 pA to 100 pA and 10 pA/step. (**c-e**), Representative traces of whole-cell

984 recordings showing electrophysiological properties of silent (n = 19), tonic-firing (n =

985 38), and bursting (n = 28) dmVMH neuronal subtypes. Three subtypes exhibit different

986 electrophysiological activity at 50, 10, and -100 pA current injection.

987

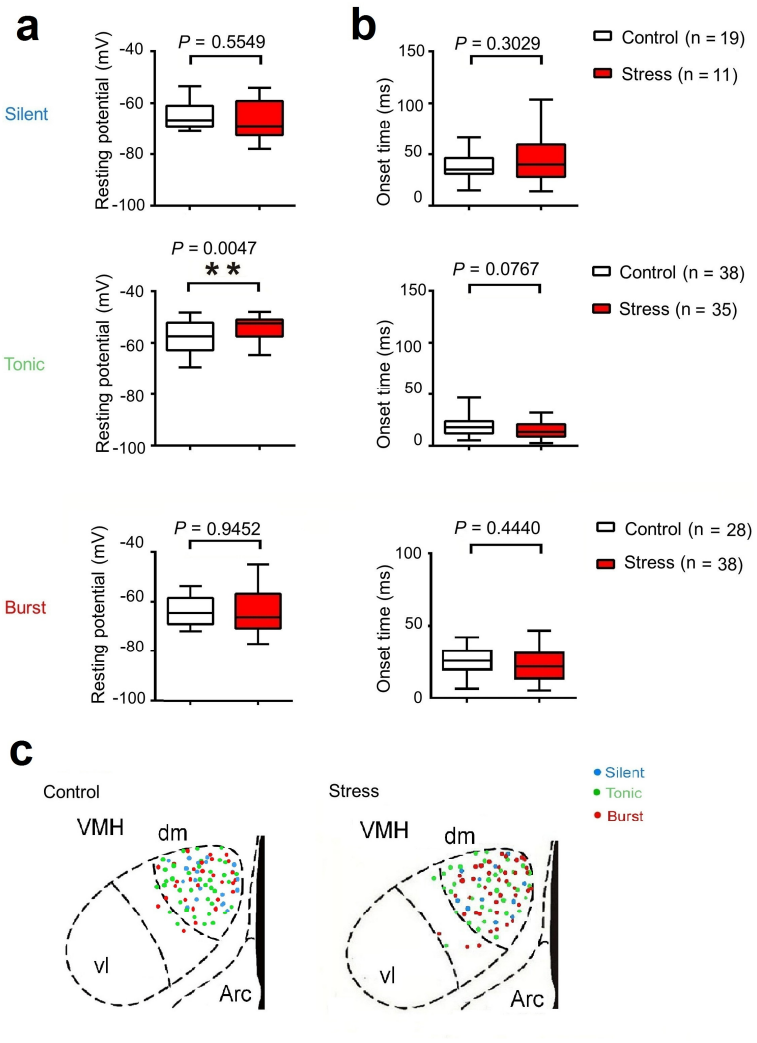


**Extended Data Fig. 2| Electrophysiological comparison of three dmVMH neuronal subtypes in control and chronic stress groups.** Related to Fig. 2.

**(a)** Resting membrane potential (RMP) of three neuronal subtypes in control and stressed mice. Top: silent neurons in control (n = 19) and chronically stress mice (n = 13), *P* = 0.5549; Middle: tonic-firing neurons in control (n = 38) and chronically stress mice (n = 33), *P* = 0.0047; Bottom: bursting neurons in control (n = 29) and chronically stress mice (n = 38), *P* = 0.9452. **(b)** Onset time of three neuronal subtypes in control and stressed mice. Top: silent neurons in control (n = 19) and chronically stress mice (n = 13), *P* = 0.3029; Middle: tonic-firing neurons in control

998 (n = 39) and chronically stress mice (n = 33), $P = 0.0767$; Bottom: bursting neurons in
999 control (n = 27) and chronically stress mice (n = 38), $P = 0.7704$ (unpaired Student's
1000 *t*-test). **(c)** Location of each recorded neuron in dmVMH of control and stressed group,
1001 no region specificity was observed among three subtypes. Data are means ± SEM; $^{*}P$
1002 $< 0.05$, $^{**}P < 0.01$. The box plotted at the median extending from the 25-75th
1003 percentile, and the whisker represents Min to Max distribution.
1004

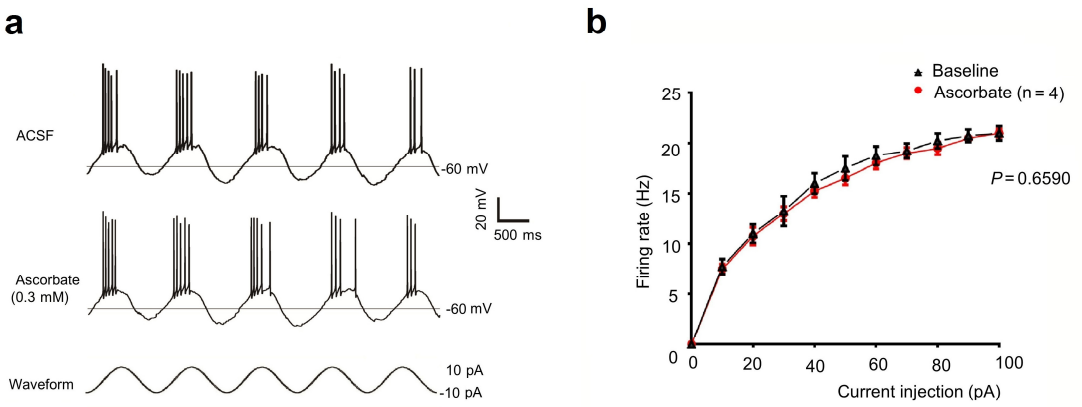


1005

1006 **Extended Data Fig. 3| Ascorbate elicited no obvious effects on burst firing in**

1007 **dmVMH neurons.** Related to Fig. 4.

1008 (**a**) Ascorbate (antagonist of Cav3.2) did not block burst firing of dmVMH neurons (n =

1009 4) induced by 10-pA current injection in cosine waveform.

1010 (**b**) Ascorbate imposed no obvious influence on burst firing of dmVMH neurons, with

1011 no significant shifts found in frequency-current curve after ascorbate application

1012 (two-way ANOVA, $P = 0.6590$, $F(1, 6) = 0.2152$ ). $^*P < 0.05$.

1013

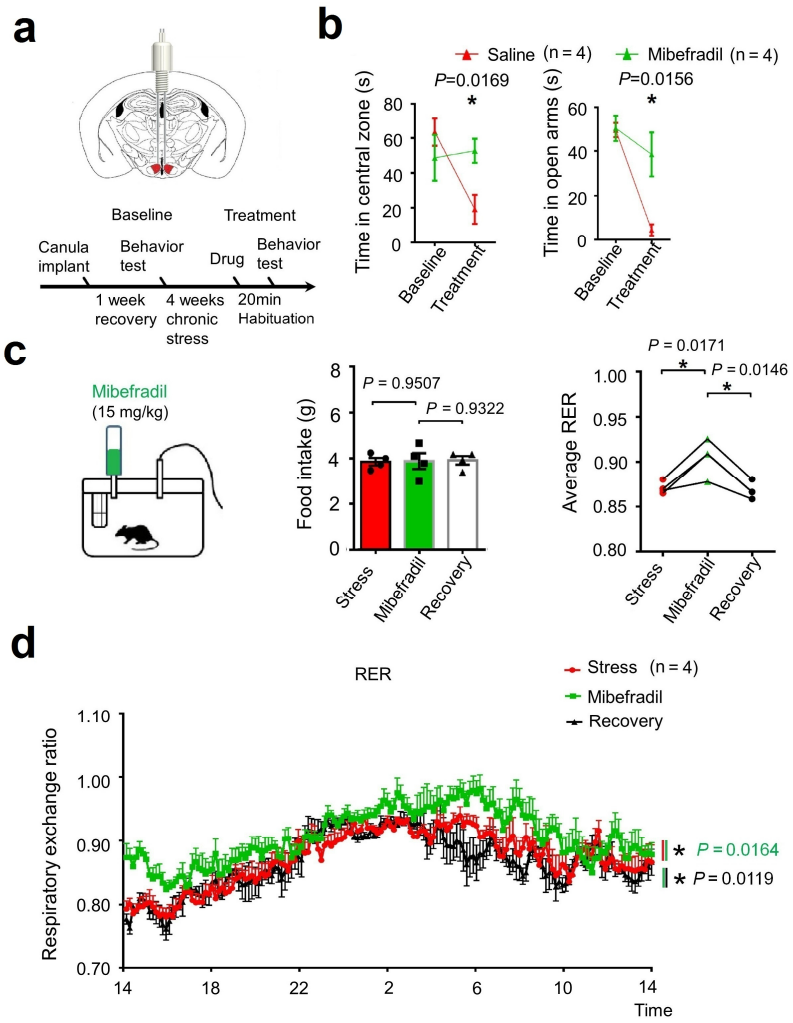


1014

1015 **Extended Data Fig. 4| Injection of T-VGCC antagonist partially ameliorated**

1016 **anxiety-like behavior**. Related to Fig. 4.

1017 **(a)** Schematic of microinjection of mibefradil in dmVMH through cannula. **(b)**

1018 Behavioral test before and after drug delivery; left, residence time in central area of

1019 open field of saline group decreased compared with mibefradil group (n = 4 in each

1020 group, $P = 0.0169$, unpaired Student's *t*-test); right, residence time in open arm of saline

1021 group decreased compared with mibefradil group (n = 4 in each group, $P = 0.0156$,

1022 unpaired Student's *t*-test). **(c-d)** Oral administration of mibefradil exerted no obvious

1023 change on food intake (n = 4 in each group, $P = 0.9507$, unpaired Student's *t*-test) but

1024 increased average RER in stressed mice ($P = 0.0171$, unpaired Student's *t*-test). Data

1025 are means ± SEM; *$P < 0.05$.

1026

1027

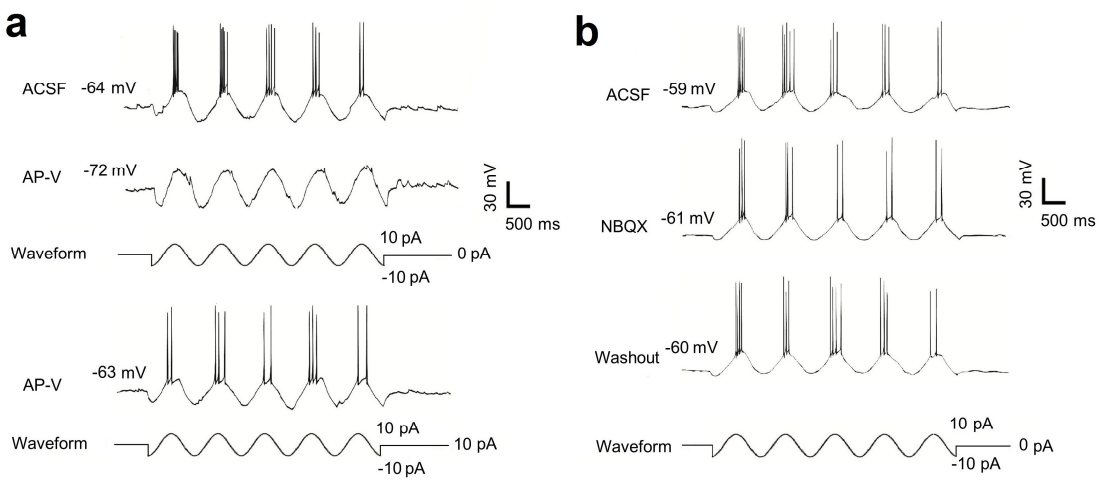


**Extended Data Fig. 5| Glutamate receptor is critical for generation of burst firing in dmVMH.** Related to Fig. 4.

**(a)** Application of APV blocked generation of burst firing induced by cosine waveform current injection (-10 pA–10 pA, n = 4), even with depolarizing current injection (10pA) to eliminate the hyperpolarization caused by APV (lower). **(b)** Application of NBQX did not abolish generation of burst firing (n = 3).

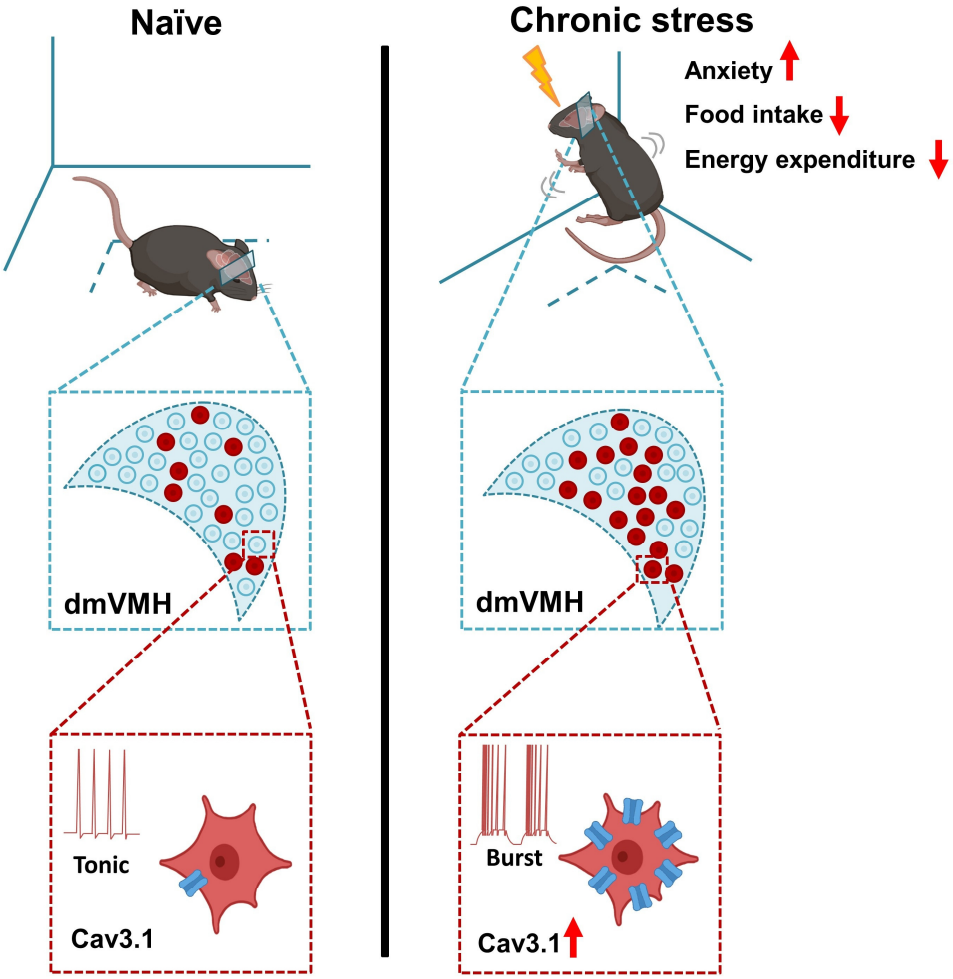


**Extended Data Fig. 6| Schematic representation of the enhancement of burst firing in dmVMH neurons after chronic stress, which was mediated by the elevated expression of Cav3.1.**